치의과학 박사학위논문

Development of absorbable magnesium bone-fixation plate

마그네슘 소재 흡수성 뼈고정판 개발

２０１７년 8월

서울대학교 대학원

치의과학과 구강악안면외과학 전공

변 수 환

Development of absorbable magnesium bone-fixation plate

마그네슘 소재 흡수성 뼈고정판 개발

지도교수 이 종 호

이 논문을 치의과학 박사학위논문으로 제출함

２０１７년 4월

서울대학교 대학원

치의과학과 구강악안면외과학 전공

변 수 환

변수환의 박사학위논문을 인준함

２０１７년 6월

위 원 장	김 명 진	(인)
부위원장	이 종 호	(인)
위 원	김 성 민	(인)
위 원	김 현 이	(인)
위 원	김 수 관	(인)

Abstract

Development of absorbable magnesium bone-fixation plate

Soo-Hwan Byun, DDS, MSD

Program in Oral and Maxillofacial Surgery, Department of Dental Science,

Graduate School, Seoul National University

(Directed by Professor Jong-Ho Lee, DDS, MSD, PhD)

Background and purpose of study

Titanium (Ti) is currently the most widely used material in bone fixation devices for craniofacial bone surgery. However, the Ti fixation device is permanent and thus increases the risk of infection due to prolonged metal exposure. Moreover, in children, there is an increased risk that the inserted fixation plate or screws will become incorporated into the bone, necessitating removal with additional surgery. Polymer-based bone fixation devices have certain advantages with respect to bioresorption; however, the strength of the polymer is still far lower than that of the Ti device.

Unlike Ti and polymer, magnesium (Mg) can provide a balance of strength and an appropriate rate of degradation. The degradation of Mg reduces the risk of long-term infection, eliminates the need for removal surgery, and can promote healing through Mg ion release. Furthermore, its elastic modulus and compressive strength are similar to those of human bone. For these reasons, Mg is being explored for various craniofacial and orthopedic applications. However, rapid degradation of Mg can cause excessive hydrogen gas formation, which can ultimately hinder clinical success. In addition, although Mg has better mechanical properties than polymer, it still has poorer mechanical properties than Ti.

The purpose of the present study was to improve the mechanical strength and control the absorption rate of Mg material and to develop an absorbable metallic plate for craniofacial application.

Methods

Chapter 1: Development and evaluation of strength-enhanced pure Mg plate

The tensile strength and flexural strength of a Ti plate and an untreated pure Mg plate were evaluated. Pure Mg plates for the in

vivo test were treated with a bi-axial rolling process to enhance the mechanical strength. Mg plates were inserted above the cranial bones of Sprague-Dawley rats (rat calvarium). In the control group (non-coated Mg group), non-coated Mg plates were inserted into 25 rats and, and five rats were sacrificed each at 2, 4, 6, 8, and 12 weeks. In the experimental group (HA-coated Mg group), hydroxyapatite (HA)-coated Mg plates were inserted into 30 rats, and five rats were sacrificed each at 2, 4, 6, 8, 12, and 24 weeks. The presence of inflammation, infection, hydrogen gas formation, wound dehiscence, and plate exposure was examined at the time of sacrifice. The absorption pattern and tensile strength of the retrieved Mg plate were examined after micro-computed tomography (μCT).

Chapter 2: Development and evaluation of Mg alloy bone-fixation plate-ZK60

Alloying is an innovative approach to improve the mechanical properties of pure Mg. In order to overcome the limitation of the poor mechanical strength of pure Mg, ZK60 was selected, which has a higher mechanical strength than pure Mg. In addition, ZK60 was

expected to be absorbed in the body fluid at a similar rate as pure Mg; poly-L-lactic acid (PLLA) coating was used to slow the absorption.

The PLLA-coated ZK60 plate was evaluated using a LeFort I osteotomy canine model of two beagle dogs. Four L-shaped plates were fixed at the anterior buttresses and posterior buttress with 16 screws. The presence of wound dehiscence, plate exposure, gas formation, occlusion, inflammation, pus formation, food intake, and fistula formation was evaluated weekly. Both dogs were sacrificed after 10 weeks, and μCT was performed. Gas formation and the absorption rate of the plates and screws were evaluated with the μCT images.

Chapter 3: Development and evaluation of Mg alloy bone-fixation plate-WE43

ZK60, which is a Mg alloy, had good mechanical properties but exhibits too rapid absorption. Thus, other types of material having slower absorption were sought. WE43 has slower absorption than ZK60. However, WE43 has low mechanical strength and is difficult

to use clinically as it requires additional strength enhancement, which can be accomplished by an extrusion process.

A WE43 Mg alloy rod was pre-treated with an extrusion process to increase its strength ("extruded WE43"). The biocompatibility of WE43 was evaluated using an osteoblast cell line (MC3T3-E1). The static immersion test in the simulated body fluid (SBF) was performed to observe the corrosion rate of the alloys over a period of 60 days. A three-point flexural test and a tensile test were performed on the Ti plate, pure Mg plate, and WE43 plate.

The extruded WE43 plate was evaluated using a LeFort I osteotomy canine model of 10 beagle dogs. Dogs were divided into two groups: five dogs in the experimental group and five dogs in the control group. Clinical evaluation was performed in the same manner as was described for the animal study using the ZK60 plate. μCT was acquired at 4, 12, and 24 weeks. The absorption of the plates and the change in the surrounding bone were evaluated. At 24 weeks after the operation, all animals were sacrificed, and histologic evaluation was performed.

Results

Chapter 1: Development and evaluation of strength-enhanced pure Mg plate

The Mg plate had lower flexural strength and tensile strength than the Ti plate. In the non-coated Mg group, gas formation and plate exposure were observed starting at 2 weeks. In the HA-coated Mg group, gas formation was not observed until 12 weeks and was also observed at 24 weeks. The HA-coated Mg group showed slower absorption of the plate compared to the non-coated Mg group. The tensile strength of HA-coated Mg plates was maintained until 12 weeks (>190 MPa).

Chapter 2: Development and evaluation of Mg alloy bone-fixation plate-ZK60

Neither of the dogs experienced any specific problem during the surgical procedure. Plate exposure, gas formation, and external fistula were not observed, and occlusion remained stable. However, the wound dehiscence that occurred after 2 weeks was not healed during the observation period. The inflammatory symptoms

continued after 2 weeks. All plates were not seen in the μCT images, and only a few screw bodies fixed in the bone remained after 10 weeks.

Chapter 3: Development and evaluation of Mg alloy bone-fixation plate-WE43

There was no difference in cell attachment or proliferation between pure Mg and WE43. The corrosion rate of WE43 remained constant for 60 days and was slow compared to that of ZK60. Approximately 60% of the initial mass remained at 60 days. The flexural strength and tensile strength of the extruded WE43 were higher than those of casted WE43.

Swelling and gas formation were observed in three dogs in the experimental groups at 8 weeks. From 12 weeks, infraorbital fistula and inflammation were observed in three dogs in the experimental group, which gradually decreased and disappeared at 24 weeks. The plate that separated from the bone showed rapid absorption, but the screw fixed inside the bone showed slow absorption. Two dogs showed less gas formation at 12 weeks compared to the other dogs. The plates were completely absorbed, and gas formation was

not observed at 24 weeks in these two dogs. In the control group, plates and screws were maintained as they were at their initial position without any problem. Osteoblastic lining and woven bone were observed around the screw threads in both groups. New bone was well formed around the plates and screws in both groups. Histologic examination showed no specific differences between the experimental group and control group.

Conclusion

The mechanical strength of pure Mg was improved by a bi-axial process; however, the tensile strength did not exceed 200 MPa. The tensile strength of ZK60 exceeded 300 MPa, but the absorption was too rapid for clinical application. The mechanical strength of extruded WE43 was sufficient for mid-facial application. Absorption of WE43 showed disadvantageous gas formation, but it was thought that the absorption rate could be optimized with a surface treatment such as coating. Plates made with appropriately treated WE43 have the potential to be useful clinically.

Keywords: Absorbable plate, Magnesium, Bone-fixation plate, Mechanical strength, Magnesium alloy, ZK60, WE43, Biocompatibility

Student number: 2012-31175

Contents

I. Background and purpose of study 13

II. Chapter I: Development and evaluation of strength-enhanced pure Mg plate 15

A. Introduction 15

B. Materials and Methods 18

1. Mechanical properties of pure Mg 18

2. Design of pure Mg plate for evaluation of strength and absorption rate 19

3. Preclinical evaluation of pure Mg plate 19

3.1. Clinical evaluation 20

3.2. Evaluation of absorption rate using μCT 21

3.3. Change of mechanical strength 21

3.4. Statistics 22

C. Results 22

1. Mechanical properties of pure Mg 22

2. Preclinical evaluation of pure Mg plate 22

2.1. Clinical evaluation 22

2.2. Evaluation of absorption rate using μCT 23

2.3. Change of mechanical strength 23

D. Discussion 24

III. Chapter 2: Development and evaluation of Mg alloy bone-fixation

plate-ZK60 24
A. Introduction 24
B. Materials and Methods 27
1. Design of ZK60 plate 27
2. Preclinical evaluation of the ZK60 plate using a Lefort I osteotomy canine model 28
2.1. Clinical evaluation 31
2.2. Evaluation of absorption rate using μCT 32
C. Results 32
1. Preclinical evaluation of ZK60 plate using a Lefort I osteotomy canine model 32
1.1. Clinical evaluation 32
1.2. Evaluation of absorption rate using μCT 33
D. Discussion 33
IV. Chapter 3: Development and evaluation of Mg alloy bone-fixation plate-WE43 34
A. Introduction 34
B. Materials and Methods 35
1. Biocompatibility and corrosion rate of WE43 plate 35
2. Mechanical properties of WE43 37
3. Design of WE43 plate for evaluation of strength and absorption rate 38
4. Preclinical evaluation of WE43 plate using a Lefort I

osteotomy canine model 39
4.1. Clinical evaluation..... 42
4.2. Evaluation of absorption rate using μCT 42
4.3. Histologic evaluation 43
C. Results 43
1. Biocompatibility and corrosion rate of WE43 plate 43
2. Mechanical properties of WE43..... 44
3. Preclinical evaluation of WE43 plate using a Lefort I osteotomy canine model 45
3.1. Clinical evaluation..... 45
3.2. Evaluation of absorption rate using μCT 45
3.3. Histologic evaluation 47
D. Discussion..... 47
V. Conclusion 52
References..... 53
Figure Legends..... 67
Figures..... 73
Tables 83
Abstract in Korean 84

I. Background and purpose of study

Titanium (Ti) is currently the most widely used type of material for bone fixation devices in craniofacial bone surgery. However, non-absorbable Ti plates and screws remain permanently in the body even after complete healing, thereby increasing the risk of infection due to prolonged metal exposure. In addition, in children, there is an increased risk that the inserted fixation plate or screws will be incorporated into the bone. Also, the elastic modulus of most metallic materials is much higher than that of human bone, which can cause stress shielding and result in bone damage. Thus, it is necessary to surgically remove the Ti fixation devices after the bone has healed.

Polymer-based bone fixation devices can degrade and be absorbed into the surrounding fluid; thus, they do not necessitate removal with additional surgery. However, they are less intense than metals. The strength of the polymer is still far lower than that of Ti. They must often be used at a larger size to compensate for their insufficient strength, and it is also difficult to control their absorption rate. As such, these polymer-based devices are used only in limited areas that are not subjected to heavy forces[1, 2].

Furthermore, studies have reported long-term foreign body reactions associated with polymeric device degradation, likely due to their acidic degradation products[3, 4].

Unlike Ti and polymer, Mg can provide a balance between strength and an appropriate rate of degradation. The degradation of Mg reduces the risk of long-term infection, eliminates the need for removal surgery, and can promote healing through Mg ion release. Also, its elastic modulus and compressive strength are similar to those of human bone[5, 6]. For these reasons, Mg is being explored for various craniofacial and orthopedic applications[7]. However, rapid degradation of Mg caused by excessive hydrogen gas formation has prevented its clinical success. In addition, although Mg has better mechanical properties than polymer, it still has poorer mechanical properties than Ti.

The purpose of the present study was to improve the mechanical strength of the Mg material, control the absorption rate, and develop an absorbable metallic plate for craniofacial applications.

II. Chapter I: Development and evaluation of strength-enhanced pure Mg plate

A. Introduction

Mg is an essential mineral in the human body. Its elastic modulus and compressive strength are similar to those of human bone, so additional removal surgery is unnecessary. Furthermore, in contrast to polymer, Mg has a 10 fold higher tensile strength and is capable of significant elongation at break. Mg is highly susceptible to corrosion in chloride-containing solutions including human body fluid or blood plasma, which limits its applications in biomaterials[8]. When Mg is exposed to the biological environment, it loses its original functionality. Furthermore, release of by-products such as hydrogen gas and hydroxide ions during Mg degradation can be harmful to the adjacent tissue and can induce alkaline poisoning and tissue necrosis[9].

$$Mg + 2H_2O \rightarrow Mg^{2+} + 2OH^- + H_2$$

McBride[10] reported in 1938 that hydrogen gas samples aspirated from a cavity 40 days after implanting a band of Mg alloy showed a gas composition of 5.6% CO_2, 6.5% O_2, 7.3% H_2, and 80.6% N_2. In

1942, McCord et al.[11] used an interferometer to analyze the compositions of gas samples drawn from sites of gas gangrene formed in rats five days after Mg powder implantation. Their results showed a gas composition of 1.3% CO_2 and 15.2% O_2, and they calculated that the H_2 concentration must have been 2.2%[11]. Kuhlmann et al.[12] reported that hydrogen must be exchanged very quickly after implantation, and it was difficult to measure the exact amount of hydrogen gas generated.

In fact, there was an attempt to promote osseointegration by incorporating Mg into dental implant. This Mg dental implant showed rapid osseointegration in comparison to the existing dental implants in a short term study[13–15]. However, peripheral bone resorption was observed clinically. The cause of this problem was suspected to be hydrogen gas formation and the change in ambient pH during the degradation process of Mg. In order to avoid such problems, the absorption should be slowed so that the metabolites are slowly absorbed into the body fluids[12].

It is important to reduce the absorption rate of Mg by all types of methods including surface reinforcement with coating[16]. Various methods of coating have been developed to reduce absorption rate

and increase the biocompatibility of Mg. A calcium-phosphate coating can improve the biocompatibility of metallic implants and increase bone growth at the site of implantation[17]. HA is the naturally occurring mineral form of calcium apatite and is a major inorganic component of natural bone[18]. It has excellent properties such as biocompatibility, absorbability, osteoconductivity, and nontoxicity[16, 19]. Other coating materials are biodegradable polymers such as poly-glycolic acid (PGA), poly-L-lactic acid (PLLA), and poly-lactic-co-glycolic acid (PLGA)[20, 21]. One of the major concerns with these coating materials is their mechanical stability, because the deformation of a Mg device can occur during surgical operations or under physiological loading conditions after implantation[22, 23]. In general, widely used biodegradable polyesters only weakly bond to Mg, which makes them susceptible to interfacial delamination under deformation; the coating layer eventually detaches, negating all benefits of the coating[24]. The purpose of this chapter was to evaluate the mechanical strength and absorption rate of a pure Mg plate, which was strength-enhanced through a bi-axial process and coated with HA.

B. Materials and Methods

1. Mechanical properties of pure Mg

A high-purity (99.99%) Mg plate and grade II Ti plate were designed (23.5x4.5 mm) for strength measurement. Pure Mg plates for evaluation of mechanical properties were not treated with any process. A three-point flexural test was conducted on the Ti plate (thickness of 0.6 mm) and pure Mg plate (thickness of 0.6 mm/0.8 mm). A three-point flexural test was carried out to measure the mechanical properties of the pure Mg plate and Ti plate. An Instron 8841 (Instron USA, Norwood, MA, USA) was used with a constant bending punch speed of 1.0 mm/min and a support distance of 12.0 mm. ASTM F382 (specification and test method for metallic bone plates) was applied as the experimental protocol. The test was stopped at the time of plate fracture. For each sample, both ends of the plate were positioned on the same horizontal plane[25]. A tensile test was also performed on the Ti plate (thickness of 0.6 mm) and the pure Mg plate (thickness of 0.6 mm/0.8 mm). Tensile strength was measured as the maximum stress that a plate could withstand while being stretched before breaking[26]. The Instron was used at a constant speed of 5.0 mm/min.

2. Design of pure Mg plate for evaluation of strength and absorption rate

High-purity (99.99%) Mg was intensified with a bi-axial rolling process for enhancing the mechanical strength. Pure Mg plates were designed (N=60, 26x6x2 mm) for strength measurement **(Figure 1)** and were mechanically polished using 1200 grit SiC paper, washed with ultrasonic washer, and then dried. Thirty-five plates for HA coating were soaked in 0.5 M ethylenediaminetetraacetic acid calcium disodium salt hydrate (Ca-EDTA) and 0.05 M potassium dihydrogen phosphate (KH_2PO_4) solution and heated at a temperature of 363 K for 2 hours. The pH was maintained at 8.9 by adding sodium hydroxide (NaOH) solution. HA-coated plates were then washed with distilled water and dried.

3. Preclinical evaluation of pure Mg plate

Fifty five 10 week old Sprague Dawley rats (body weight of 300-350 g) were randomly divided into two groups after a 2 week adaptation period. Non-coated Mg plates (non-coated Mg group) were inserted into 25 rats, and HA-coated Mg plates (HA-coated Mg group) were inserted into 30 rats (rat calvarium). General

anesthesia with a mixture of xylazine (Rompun®, 20 mg/ml, Bayer Korea Ltd., Korea) and ketamine hydrochloride (Ketalar®, 50 mg/ml, Yuhan Corp., Korea) (1:4 volumes, dosage 0.15 ml/100 g) was injected intraperitoneally. The cranial hair was shaved, and the skin was sterilized with a povidone-iodine sponge. A transverse skin incision was made, and the periosteum was elevated using the periosteal elevator. The Mg plate was inserted carefully underneath the periosteum, and the flap was sutured using 5-0 nylon (Ethicon®, Johnson & Johnson, New Brunswick, NJ, USA) **(Figure 2)**. Five rats were sacrificed using CO_2 asphyxiation each at 2, 4, 6, 8, and 12 weeks in the non-coated Mg group, and five rats each were sacrificed at 2, 4, 6, 8, 12, and 24 weeks in the HA-coated Mg group.

3.1. Clinical evaluation

The presence of inflammation, infection, gas formation, wound dehiscence, and plate exposure was examined at the time of sacrifice. The Mg plates were retrieved, and the absorption pattern was examined.

3.2. Evaluation of absorption rate using μCT

μCT (Skyscan 1172 Micro-tomography System, Skyscan, Kontich, Belgium) was performed, and the absorption rate and pattern of the Mg plate were examined. The volume was constructed with the sectioned images using the Feldkamp algorithm. The computation for absorption rate (DRi) is shown below.

$$DRi=\frac{Vi}{V}X100 \ , \ Vi=V-Vci$$

Sectioned images of the plates before the experiment with μCT were constructed three-dimensionally (V) using the CTvox program (Skyscan, Kontich, Belgium). The volume at the time of sacrifice (Vi) is the volume of the plate before the experiment (V) minus the measured volume of the constructed three-dimensional absorbed area (Vci).

3.3. Change of mechanical strength

The Mg plate was retrieved after μCT. The tensile strength of the retrieved Mg plate was measured using a universal testing machine (OTU-05D, Oriental TM Corp., Korea) with a crosshead speed of 1 mm/min.

3.4. Statistics

The absorption rate and tensile strength of the Mg plate were analyzed using Student's t-test, two-way analysis of variance (ANOVA), and repeated measurement ANOVA and confirmed with Bonferroni's multiple comparison test ($p<0.05$) using the SPSS 22.0 program (IBM SPSS Statistics, IBM Corp., Somers, NY).

C. Results

1. Mechanical properties of pure Mg

There was no difference in flexural strength according to the thickness of the Mg plate. The Ti plate had 2.5 times higher flexural strength than the Mg plate of the same thickness (0.6 mm) and 2.4 times higher than the Mg plate of 0.8 mm thickness (Figure 3A). There was no difference in tensile strength according to Mg plate thickness. The tensile strength of the Ti plate was more than 300 MPa, and that of the Mg plate was just over 100 MPa (Figure 3B).

2. Preclinical evaluation of pure Mg plate

2.1. Clinical evaluation

All rats recovered immediately after surgery. Clinical examination

showed no specific findings up to 1 week postoperative. In the non-coated Mg group, gas formation and plate exposure were observed starting at 2 weeks. In the HA-coated Mg group, gas formation was not observed until 12 weeks. Gas formation was still observed at 24 weeks, and plate exposure was not observed in the HA-coated Mg group. The corrosion products were covering the surface of the non-coated Mg plates starting at 2 weeks. The HA-coated Mg plates showed no specific change until 2 weeks, but the coating started to strip off and assume a pin-point-like appearance at 4 weeks that gradually progressed until 12 weeks **(Figure 4)**.

2.2. Evaluation of absorption rate using μCT

The HA-coated Mg plate showed statistical significance (p<0.001) in the resistance to absorption, demonstrating slower absorption than the non-coated Mg group. The absorption of the HA-coated Mg plate had progressed significantly at 12 weeks **(Figures 5 and 6)**.

2.3. Change of mechanical strength

The tensile strength of the HA-coated Mg plates was maintained until 12 weeks (>190 MPa). However, the tensile strength of the non-coated Mg plates decreased significantly starting at 2 weeks (p<0.05), and the strength continuously decreased significantly with

time (p<0.05) **(Figure 6)**. The tensile strength of the plates did not exceed 200 MPa.

D. Discussion

Preclinical evaluation confirmed the effects of HA coating for controlling the absorption rate. During the observation period of 24 weeks, the non-coated Mg group showed gas formation and plate exposure from 2 weeks, while the HA-coated Mg group did not show gas formation and plate exposure until 12 weeks. This indicates that the HA coating is biocompatible and resistant to corrosion in vivo. Bi-axial processing was performed to increase the mechanical strength of pure Mg, but the tensile strength did not exceed 200 MPa during the evaluation period. Thus, future research is needed to overcome these limitations.

III. Chapter 2: Development and evaluation of Mg alloy bone-fixation plate-ZK60

A. Introduction

Alloying is an innovative approach to improve the mechanical

properties of pure Mg, and it should be considered in the case of Mg alloys for biomedical applications. Most Mg alloys that have been investigated as potential implant materials are rather complex in alloy composition and contain potentially toxic alloying elements[5]. For alloys containing rare earth metal elements such as yttrium, controversy exists as to their biological effects[27, 28]. In principle, elements with potential toxicological problems should be avoided or used in the minimal acceptable amounts in the selection of biodegradable material. In this present research, ZK60 and WE43 were chosen as biodegradable Mg alloys to evaluate their performance in bone fixation plates (Table 1).

Zinc (Zn) of ZK60 is a common alloying ingredient in Mg and has a good strengthening effect[29]. It aids in overcoming the harmful corrosive effect of impurities such as iron and nickel, thus improving the corrosion resistance of the Mg alloy. Its concentration is usually limited to 3% for good corrosion resistance[29]. Zirconium (Zr) of WE43 is usually used as a grain refiner in Mg alloys, contributing to the strength of the Mg alloy[29]. It also reduces the adverse effects of iron contaminant on the corrosion resistance of Mg alloys. In the Mg–Zr binary alloy system,

Zr is effective at enhancing corrosion resistance only when its content is less than 0.48% with no formation of Zr-containing precipitates[30]. While the importance of Zr in the human body is still being determined, it has been reported that Zr shows good biocompatibility and osseointegration both in vitro and in vivo, even outperforming Ti[31].

The mechanical strength of ZK60 and WE43 is higher than that of pure Mg, and the strength of ZK60 is higher than that of WE43. The elongation rate of ZK60 is also higher than that of WE43 (Table 2). The degradation behavior of ZK60 was investigated in terms of ion release and pH value of non-static Hank's solution over a period of seven days[29]. Its biocompatibility was evaluated by testing cell viability in vitro under the influence of the eluate of the material[29]. A comparison was made with a WE-type alloy as well as with HA in order to establish the viability of the ZK-type alloy as a potential biodegradable material for biomedical applications[29]. It was found that, at the tested concentration of the extract, ZK-type and WE-type alloy samples displayed biocompatibilities similar to that of HA after 1 day of incubation[29]. Thus, the biocompatibility of ZK60 and WE43 has been demonstrated, and both Mg alloys have better

mechanical strength than pure Mg.

In order to overcome the limitation of the mechanical strength of pure Mg, ZK60 was first selected, which has higher mechanical strength than WE43. In addition, ZK60 was expected to absorb rapidly in the body fluid, similar to pure Mg, so a PLLA coating was used to slow the absorption. The purpose of this chapter was to evaluate the mechanical strength and absorption rate of a ZK60 plate coated with PLLA in a LeFort I osteotomy canine model.

B. Materials and Methods

1. Design of ZK60 plate

ZK60 (Daeryun Co., Shanghai, China) was used to fabricate the plates and screws. Mg alloy plates were made to be slightly thicker and larger than the conventional Ti plates. L-shaped plates with four holes were designed. Mg alloy plates with a thickness of 1.0 mm and an outer hole size of 5.5 mm were prepared with a milling machine (Genoss Co., Suwon, Korea) (Figure 7). The plates were soaked in a PLLA-polymer solution (5.0 wt% dissolved in dichloromethane) for 5 minutes under vacuum pressure at 0.05 MPa. To form the PLLA layer, using a dip coater, the plates were

vertically withdrawn from the solution at a rate of 65 mm/min[32]. The PLLA-coated plates were rinsed with ethanol and dried in air. The screws were designed to have a self-threading cutting edge to reduce the insertion torque. Mg alloy screws with dimensions of 6.0 mm in length and 3.4 mm in diameter were prepared with a milling machine (Figure 7). Before implantation, all of the Mg devices were cleaned using sonication in pure acetone and ethanol for 10 minutes each and were sterilized with gamma radiation ($2*10^6$ cGy, 23.5 Gy per minute).

2. Preclinical evaluation of the ZK60 plate using a Lefort I osteotomy canine model

Two 20 month old beagle dogs (10-15 kg body weight) (Oriental Bio Co, Korea) first underwent a 4 week adaptation period. Their front paw hair was shaved, and the bare paw was sterilized with a povidone-iodine sponge, followed by insertion of an intravenous catheter line in the vein with a 24-gauge needle. General anesthesia was administered intravenously with xylazine 0.1-0.14 ml/kg (Rompun®, 23.32 mg/ml, Bayer Korea Ltd., Korea) and

tiletamine+zolazepam 0.01 mg/kg (Zoletil®, 50 mg/ml, Virbac Corp, France), and orotracheal intubation was performed using size 6 tubes without ballooning for securing the airway. The tube was fixed to the anterior part of the mandible using paper tape, and the fixed part was marked so that the position of the tube was consistent. The oral cavity was disinfected with chlorhexidine gauze and a toothbrush and was sterilized with another povidone-iodine sponge. The infraorbital foramen was identified with tactile sensation. Block and infiltration anesthesia was performed intraorally with 2% lidocaine[33].

A sulcular incision was made from the upper incisor region to the upper second molar region using a #15 blade. Unexpected hemorrhage was coagulated using a bipolar coagulator (Martin, Germany) and oxidized regenerated cellulose (Surgicel®, Johnson & Johnson, USA). Periosteal elevation was performed posteriorly with minimal damage from the upper second molar to the maxillary tuberosity. The infraorbital nerve exposed during the periosteal elevation was further anesthetized using 2% lidocaine. When hemorrhage occurred, additional hemostasis was performed using a

hemostatic agent (Avitene®, Davol Inc., UK). A LeFort I osteotomy line was drawn using a pencil. The osteotomy line was planned from the top of the piriform aperture to the second molar apex (**Figure 8A**). Four L-shaped plates were fitted at both anterior buttresses on the canine site and the posterior buttress on the upper site of the third premolar[34]. When fitting the plates, the screws were positioned to avoid the osteotomy line. After the plates were fitted, 16 holes were made on the bone with a 1.5-mm-sized drill at a speed of 1500 rpm (Dentium, Suwon, Korea) and sufficient saline irrigation. Plates were fixed using 16 screws. Then, the four plates and 16 screws were removed. The LeFort I osteotomy was performed carefully on the maxillary tuberosity area using a reciprocating saw to ensure that the periosteum was not damaged **(Figure 8B)**. Severe hemorrhage around the osteotomy line was managed with a hemostatic agent (Ostene®, Baxter, USA) for hemostasis. The operator confirmed a complete anteroposterior fracture. The separated maxillary bone was repositioned after hemostasis, and the four plates and 16 screws were fixed to the preformed holes (**Figure 8C**). Copious irrigation and interrupted

sutures were performed using 4−0 nylon sutures (Dafilon®, Braun, Germany). A laryngoscope was used to check and aid in the removal of blood clots and other remaining residues in the larynx or mouth. Orotracheal intubation was not concluded until complete recovery from general anesthesia. Pulverized feed was given in the same amounts as before surgery for 4 weeks after the operation. Analgesics (0.2 mg/kg, Meloxicam, Hanall, Korea) and antibiotics (30−60 mg/kg, Cephalexin cap, Ildong, Korea) were mixed with the pulverized feed and were given for up to seven days after surgery. After 4 weeks, a regular diet was provided.

2.1. Clinical evaluation

The presence of wound dehiscence, plate exposure, gas formation, inflammation, pus formation, occlusion, food intake, and fistula formation was evaluated weekly. Occlusion was evaluated with photographs taken before and after the experiment. The mobility and stability of the maxilla were evaluated by an examiner by holding the cranial bone with the left hand and the anterior portion of the maxilla with the right hand and shaking it back and forth. Mobility was classified into three groups: 2= great mobility, 1= little mobility, and 0=no apparent mobility.

2.2. Evaluation of absorption rate using μCT

After 10 weeks, both dogs were sacrificed, and μCT (SkyScan1173; SkyScan, Kontich, Belgium) was performed. Gas formation and the absorption rate of the plates and screws were evaluated with μCT images.

C. Results

1. Preclinical evaluation of ZK60 plate using a Lefort I osteotomy canine model

1.1. Clinical evaluation

Neither dog encountered any specific problems during the surgical procedure. Plate exposure, gas formation, and external fistula were not observed, and occlusion remained stable. However, the wound dehiscence that occurred at 2 weeks did not heal during the observation period **(Figure 9A)**. The inflammatory symptoms continued after 2 weeks **(Figure 9B)**. Instability of the maxilla was not observed, and there was no difference in food intake during the observation period.

1.2. Evaluation of absorption rate using μCT

Gas formation was not observed on the CT images acquired at 10 weeks, and all plates were not seen in both dogs (Figure 9C). Only a few screw bodies fixed in the bone remained, and the screw heads were completely absorbed after 10 weeks (Figure 9D).

D. Discussion

The PLLA-coated ZK60 plate was absorbed in just 10 weeks, which caused an inflammatory response due to rapid absorption. Although ZK60 has better mechanical properties than WE43, it is known that its absorption is faster when it comes into contact with body fluid. ZK60 was significantly degraded in 9 weeks and was completely degraded after 12 weeks[29].

In previous research, the general long-term absorption behavior of WE-type and ZK-type alloys was evaluated by static immersion test in which the concentration of chloride ions was maintained at a constant level[29]. Such a static immersion system cannot exactly simulate the actual physiological conditions in the human body because the body fluid circulates dynamically, and ion concentrations differ in different parts of the human body[35].

Nevertheless, the local concentration of chloride ions is one of the most important factors that determine the absorption rate of Mg alloys when they are exposed to an aggressive electrolyte such as simulated body fluid or sodium chloride solution. Different behavior in absorption rate has been revealed[35].

The absorption rate of Mg alloy must not exceed the healing rate of the bone. Thus, the Mg alloy should remain in the body and maintain its mechanical integrity for at least 12–18 weeks while the bone tissue heals[28]. The results from the present study suggest that the absorption rate of the ZK60 plate was too fast despite the PLLA coating. Therefore, further optimization of plates made with Mg alloy is needed to achieve an appropriate rate of absorption.

IV. Chapter 3: Development and evaluation of Mg alloy bone-fixation plate-WE43

A. Introduction

Pure Mg has insufficient mechanical strength for clinical application. ZK60, which is a Mg alloy, had good mechanical properties but exhibits excessively rapid absorption in vivo. WE43, one of the Mg

alloys, has slower absorption than ZK60 (Table 2)[29], but it has insufficient mechanical strength to be useful in the clinic. However, the extrusion process and other additional strength enhancement techniques can increase the mechanical strength by approximately 15–20% to obtain a strength similar to that of ZK60. Herein, the biocompatibility and absorption rate of extruded WE43 were assessed to determine whether it is suitable for preclinical evaluation.

In this chapter, the biocompatibility and absorption rate of extruded WE43 were evaluated. A plate was designed based on an in vitro test and was then applied in animal models for preclinical evaluation.

B. Materials and Methods

A WE43 Mg alloy rod was pre-treated with an extrusion process to increase its strength (Daeryun Co., Shanghai, China) (extruded WE43) (Tables 1,2).

1. Biocompatibility and corrosion rate of WE43 plate

The rods were cut into disks with a diameter of 28 mm and a thickness of 5 mm. The biocompatibility of the WE43 alloy was

evaluated using a pre-osteoblast cell line (MC3T3-E1). The pre-incubated cells were seeded on disks at a density of $5.0x10^4$ cells/mL and cultured in α-minimum essential medium (Welgene Co., Korea) by adding 10% fetal bovine serum and 1% penicillin streptomycin in a humidified incubator under an air atmosphere containing 5% CO_2 at 37° C. After 1 day of culturing, the cell response was observed under SEM (x1000, 20 kV, JSM-5600, JEOL). Prior to the SEM observations, the samples were fixed with 2.5% glutaraldehyde for 10 minutes, dehydrated with graded ethanol (70, 90, 95, and 100% ethanol in sequence), immersed in hexamethyl-disilazane for 10 minutes, and then air dried.

A long-term static immersion test in simulated body fluid (SBF) was performed to observe the degradation behavior of the alloys over 60 days[36]. The tests were performed at a pH of 7.35 and 37.0° C in a thermostatic bath. For each of the five disks, 30 ml of SBF solution was used. During the testing period of 60 days, the whole immersion system was regularly refilled with deionized water to a level of 30 ml in order to compensate for the liquid loss due to evaporation in the ambient atmosphere. The remaining mass was measured once a week.

2. Mechanical properties of WE43

A three-point flexural test was performed on a Ti plate (thickness of 0.5 mm), a pure Mg plate (thickness of 1.6 mm), casted WE43 (thickness of 1.2 mm), and extruded WE43 (thickness of 1.0 mm). An Instron 8841 (Instron USA, Norwood, MA, USA) with a 2 kN load capacity was used with a constant bending punch speed of 1.0 mm/min and a support distance of 12.0 mm. ASTM F382 (specification and test method for metallic bone plates) was applied as the experimental protocol. The test was stopped at the time of fracture. For each sample, both ends of the plate were positioned on the same horizontal plane with two lower stabilizing points[25]. A tensile test was also performed on the Ti plate (thickness of 0.5 mm), the pure Mg plate (thickness of 1.0 mm), the casted WE43 (thickness of 1.0 mm), the extruded WE43 (thickness of 1.0 mm), and the extruded WE43 (thickness of 1.2 mm). Tensile strength was measured as the maximum stress that a plate could withstand while being stretched before breaking[26]. An Instron 8841 was used with a constant speed of 5.0 mm/min.

3. Design of WE43 plate for evaluation of strength and absorption rate

Extruded WE43 was used to fabricate the plates and screws. All devices were designed to accommodate the maxillary geometry of the beagle dog. Plates were made to be slightly thicker and larger than the Ti plates (**Figure 10**). The plates were designed to be L-shaped with four holes. Using a milling machine, the plates were prepared with a 4.5 mm inter-hole distance, 1.0 mm thickness, and 4.5 mm outer hole size **(Figure 10A)**. The screws were designed to have a self-threaded cutting edge to reduce insertion torque. Screws with dimensions of 6.0 mm in length and 2.0 mm in diameter were prepared with a milling machine **(Figure 10A)**. Before implantation, all of the Mg devices were cleaned using sonication in pure acetone and ethanol for 10 minutes each and were sterilized with gamma radiation ($2*10^6$ cGy, 23.5 Gy per minute).

For the control group, Ti plates and screws were obtained from a DENTIUM CMF Plate System kit® (Genoss Co., Suwon, Korea). Plates were prepared to be L-shaped with four holes. Using a milling machine, Ti plates were prepared with a 4.5 mm hole distance, 0.4 mm thickness, 3.5 mm outer hole, and 1.7 mm inner

hole (Figure 10B). Ti screws with dimensions of 6.0 mm in length, 1.6 mm in diameter, and 2.5 mm in head diameter were prepared with a milling machine (Figure 10B). Ti devices were sterilized by steam sterilization.

4. Preclinical evaluation of WE43 plate using a Lefort I osteotomy canine model

Ten 20 month old beagle dogs (10–15 kg body weight) were allowed a 4 week adaptation period and then separated into two groups. WE43 plates and screws were used in the experimental group (five dogs), and the Ti plate and screws were used in the control group (five dogs). Their front paw hair was shaved, and the paw was sterilized with a povidone–iodine sponge, followed by insertion of an intravenous catheter line in the vein with a 24–gauge needle. General anesthesia was administered intravenously with 0.1–0.14 ml/kg xylazine and 0.01 mg/kg tiletamine+zolazepam. Orotracheal intubation was performed using size 6 tubes without ballooning for securing the airway. The tube was fixed to the anterior part of the mandible using paper tape, and the fixed part was marked so that the position of the tube remained constant. The

oral cavity was disinfected with chlorhexidine gauze and a toothbrush and was sterilized with the povidone-iodine sponge. The infraorbital foramen was identified with tactile sensation. Block and infiltration anesthesia was performed intraorally with 2% lidocaine[33].

A sulcular incision was performed from the upper incisor region to the upper second molar region using a #15 blade. Unexpected hemorrhage was coagulated using a bipolar coagulator and oxidized regenerated cellulose. Periosteal elevation was performed posteriorly with minimal damage from the upper second molar to the maxillary tuberosity. The infraorbital nerve exposed during the periosteal elevation was further anesthetized using 2% lidocaine. When hemorrhage occurred, additional hemostasis was performed using a hemostatic agent. A LeFort I osteotomy line was drawn using a pencil. The osteotomy line was planned from the top of the piriform aperture to the second molar apex **(Figure 8A)**. Four L-shaped plates were fitted at the anterior buttresses on the canine site and the posterior buttress on the upper site of the third premolar[34]. When fitting the plates, the screws were positioned to avoid the osteotomy line. After the plates were fitted, 16 holes were made on the bone using a 1.5-mm drill (Dentium, Suwon,

Korea) at a speed of 1500 rpm with sufficient saline irrigation. Plates were fixed using 16 screws. Then, the four plates and 16 screws were removed. The LeFort I osteotomy was performed carefully, including the maxillary tuberosity area, using a reciprocating saw to ensure that the periosteum was not damaged (Figure 8B). Severe hemorrhage around the osteotomy line was managed with a hemostatic agent. The operator confirmed complete anteroposterior fracture. The separated maxillary bone was repositioned after hemostasis, and four plates and 16 screws were fixed to the preformed holes (Figure 11). After complete fixation, the mobility and stability of maxilla were checked with the same method mentioned previously. Copious irrigation and interrupted suture were performed using 4-0 nylon sutures (Dafilon, Braun, Germany). A laryngoscope was used to check and aid in the removal of blood clots and other remaining residues in the larynx or mouth. The orotracheal intubation tube was not removed until complete recovery from general anesthesia. Pulverized feed was given in the same amounts as before surgery for 4 weeks after the operation. Analgesics and antibiotics were mixed with the pulverized feed and were given for up to seven days after surgery.

After 4 weeks, the general diet was provided.

4.1. Clinical evaluation

The presence of oral wound dehiscence, plate exposure, gas formation, inflammation, pus formation, occlusion, food intake, and fistula formation was evaluated weekly until 24 weeks. Occlusion was evaluated using photographs taken before and after the experiment. The mobility and stability of maxilla were evaluated by an examiner by holding the cranial bone with the left hand and the anterior portion of the maxilla with the right hand and shaking it back and forth. Mobility was classified into three groups: 2= great mobility, 1= little mobility, and 0=no apparent mobility.

4.2. Evaluation of absorption rate using μCT

μCT (SkyScan1173; SkyScan, Kontich, Belgium) was performed at 4, 12, and 24 weeks under general anesthesia. The absorption of the plates and the change in the surrounding bone were evaluated.
In addition, the volume of the remaining screw fixed in the bone was calculated by combining 7.1 μm cross-sectional cuts of μCT images of the remaining amount of the screw and the amount of cortical and marrow bone including 1 mm around the circumference of the screw

and were constructed three-dimensionally using CT analysis software.

4.3. Histologic evaluation

At 24 weeks after the operation, all animals were sacrificed with 7.5 mg/kg tiletamine+zolazepam. After sacrifice, the maxilla was fixed in 10% neutral buffered formalin solution, decalcified, and stained with hematoxylin & eosin (H&E) and Masson's trichrome (MT). The absorption of plate and screws, changes in the surrounding bone, inflammatory response, and bone formation were evaluated. The anterior and posterior positions of the plate were confirmed with the μCT image and were sectioned accordingly (Figure 12).

C. Results

1. Biocompatibility and corrosion rate of WE43 plate

A few cells were found on the surface of the WE43. There was no difference in cell attachment between pure Mg and WE43 (Figure 13). The amount of mass loss with the WE43 samples during the static immersion test is shown in Figure 14. The absorption rate

remained constant for 60 days and was slower than that of ZK60. Approximately 60% of the initial mass remained at 60 days.

2. Mechanical properties of WE43

In a three-point flexural test, the results were different according to the type of material in the plate and its processing method. The flexural strength of WE43 was higher than that of pure Mg, and that of the extruded WE43 was higher than that of casted WE43. The outcome of the tensile test was similar to that of the three-point flexural test. The tensile strength of the pure Mg plate (thickness of 1.0 mm) was lower than that of the Ti plate (thickness of 0.5 mm), but that of the casted WE43 plate (thickness of 1.0 mm) was higher. The extruded WE43 plate showed higher strength than the casted WE43 plate with the same thickness.

Based on these results, a 0.4 mm Ti plate was used for the control group, and a 1.2 mm Mg alloy plate was used for the experimental group **(Figure 10)**. The strength of the Mg alloy was increased through an extrusion process, and the thickness was increased so that the strength was higher than that of the Ti plate in order to prevent fracture and tear.

3. Preclinical evaluation of WE43 plate using a Lefort I osteotomy canine model

3.1. Clinical evaluation

All dogs showed stable outcomes without any specific problems. After the operation, the stability of the maxilla was measured at '0,' the same as before the operation in all dogs. In the control group, there were no particular problems during the operation. On the 10th postoperative day, dehiscence was observed intraorally in the second dog of the experimental group and the fifth dog of the control group. Additional sutures were performed on the area. No dehiscence was observed intraorally until 24 weeks except for the dehiscence observed in the above mentioned dogs **(Figure 15)**.

Swelling and gas formation were observed in three dogs of the experimental groups starting at 8 weeks. Infraorbital fistula and inflammatory symptoms were observed in three dogs of the experimental groups starting at 12 weeks, which gradually decreased and disappeared at 24 weeks **(Figure 16)**. Occlusion remained stable until 24 weeks.

3.2. Evaluation of absorption rate using μCT

No specific findings were observed at 4 weeks in the experimental

group. Gas formation was observed in three dogs of the experimental group at 12 weeks, but not at 24 weeks. All of the plates in the experimental group were well maintained until 12 weeks and mostly absorbed at 24 weeks (Figure 17). The plates separated from the bone and showed rapid absorption, but the screws fixed inside the bone showed slow absorption. Two dogs showed less gas formation at 12 weeks compared to the other dogs. The plates were completely absorbed at 24 weeks in these two dogs. The LeFort I osteotomy line in the experimental group disappeared at 24 weeks (Figure 18). In the control group, plates and screws were maintained as at the initial position without any problem. The osteotomy line was clearly visible at 4 weeks and had slightly disappeared at 12 weeks. At 24 weeks, the osteotomy line was not observed, and complete bone healing was observed (Figure 19).

In the evaluation of the absorption rate using μCT images, all plates deviated from their original position as they were absorbed. It was difficult to overlay the plates. Thus, only 10 screws that remained in the original position were evaluated. As a result, 19.37% of the initial volume remained after 24 weeks. The new bone was

measured to be approximately 10.97 mm^3.

3.3. Histologic evaluation

Histologically, there was no inflammation in any of the both groups (Figure 20). Soft tissue formation between the screw and bone was not found. An osteoblastic lining and woven bone were observed around the screw threads. New bone was well formed near the screw head and covered the screw body (Figure 20A) in the experimental group. New bone was well formed around the plates and screws, as seen in MT staining images in both groups (Figure 20B). Histologic examination showed no specific differences between the experimental group and control group.

D. Discussion

The WE43 plate had sufficient mechanical strength. The extrusion process and changes in the plate design definitely increased the strength of the WE43 plates[37, 38]. Although additional tests should be performed to evaluate the biocompatibility and mechanical strength, these results demonstrate the possibility of WE43 for clinical application[39]. Mg and its alloys have been suggested as proper materials for medical implants[5, 40]. Mg and its alloys are

promising materials for degradable implants due to their properties[41]. For example, Mg is one of the most abundant elements in the human body and an important mineral in human metabolism, together suggesting that release of Mg ions would not be harmful but might actually promote bone tissue growth[16, 41]. Not only the tissues around the screws, but also tissues in the lungs, liver, intestines, kidneys, pancreas, and spleen showed no histological abnormalities in other studies using Mg alloy implants[42-45]. Mechanical properties of Mg are similar to human bone, so the risk of stress shielding is mitigated[16]. In addition, Mg has been shown to improve the osteogenic differentiation of cells and indirect bone formation[46-48].

In this present study, swelling was observed starting at 8 weeks, and hydrogen gas was likely generated. A large amount of hydrogen gas means that the absorption of Mg was too rapid. To overcome this, it is necessary to find a way to slow the absorption. Many methods have been studied to reduce the rapid corrosion of Mg such as alloying and surface modification[5, 28, 49-54]. Surface modification with protective coatings can be applied to extend the absorption period, as mentioned above[55-57]. Controlling the

absorption rate means that the rate of hydrogen gas formation can be controlled as well[16]. If the rate of hydrogen gas formation is slowed, the generated hydrogen gas can be absorbed into the body fluid, and swelling and fistula formation can be prevented. Control of the absorption rate using carefully engineered coatings has been described in other studies[56–58].

According to a recently published paper by Lim et al.[59], there was not a difference in the absorption rate of coated WE43 at 6 and 12 weeks. In reference to this study, the present study used non-coated WE43 because the absorption can be too slow with the coating. However, there were some differences between the present study and the study of Lim et al.[59] First, Lim et al.[59] used screws only. If only screws are used (no plate), the total Mg volume is relatively small compared to the use of both screws and a plate. Therefore, hydrogen gas formation was lower than the present study. Second, the screw head was the first to be absorbed, and the plate was separated from the screw and bone in this study. As the separated plate deviated from its original position, there was increased contact with the body fluids, and absorption took place faster than with the screws that were fixed in the bone. Because of

this, a larger amount of hydrogen gas was generated during the early stage. Third, screw placement was performed without osteotomy in the study of Lim et al.[59], and LeFort I osteotomy was performed in the present study. When the osteotomy was performed, there was bleeding; as body fluid increased, absorption of Mg was accelerated. These could be the reasons for the differences between the results of Lim et al.[59] and ours.

The absorption rate of Mg can be adjusted by manipulating the coating of the WE43 alloy in further studies. There are many ways to coat plates, and HA coating has shown promise[16, 21, 60-68]. HA coating increases the biocompatibility of Mg and contributes to bone formation by increasing osteoblast attachment[9, 41, 69, 70]. The first site of absorption was the screw head, and the site that remained until late was the screw body[9]. This suggests that the body fluid of bone marrow does not actively absorb Mg, but the area directly underneath the mucosa seems to absorb rapidly due to external movement and dynamic flow of body fluid. In further studies on coatings, the screw head with the fastest absorption should be thicker and have a denser coating than the screw body.

The Mg alloy plate and screw used in this present study were

larger than the plate and screw used in the control group. Various methods have been studied to increase the strength of Mg, but pure Mg showed poor strength even after processing[37, 38]. Alloying can also increase strength. Many Mg alloys have higher strength than pure Mg but no difference in biocompatibility[71–74]. In order to increase the strength of WE43, an extrusion process was performed, but the obtained strength did not reach that of the Ti of the same size. Similar results were obtained by increasing the size and thickness of WE43 plate and screw by approximately 70–100%.

The WE43 plates and screws used herein were 50–70% larger than the Ti plate. However, the size of the plates and screws should be adjusted based on our results. The Ti plates and screws used in the control group had sufficient strength to be used in humans. In relation to the reduced size of the Ti plates and screws, the size of the Mg plates and screws can be reduced accordingly.

V. Conclusion

The mechanical strength of pure Mg was improved by a bi-axial process; however, the tensile strength did not exceed 200 MPa. The tensile strength of ZK60 exceeded 300 MPa, but the absorption was too rapid for clinical application. The mechanical strength of extruded WE43 was sufficient for mid-facial application. Absorption of WE43 showed disadvantageous gas formation, but it was thought that the absorption rate could be optimized with a surface treatment such as coating. Plates made with appropriately treated WE43 have the potential to be useful clinically.

References

1. Dolanmaz D, Uckan S, Isik K, Saglam H. Comparison of stability of absorbable and titanium plate and screw fixation for sagittal split ramus osteotomy. Br J Oral Maxillofac Surg 2004; 42: 127–132.
2. Esen A, Ataoglu H, Gemi L. Comparison of stability of titanium and absorbable plate and screw fixation for mandibular angle fractures. Oral Surg Oral Med Oral Pathol Oral Radiol Endod 2008; 106: 806–811.
3. Bostman O, Hirvensalo E, Makinen J, Rokkanen P. Foreign–body reactions to fracture fixation implants of biodegradable synthetic polymers. J Bone Joint Surg Br 1990; 72: 592–596.
4. Weiler A, Helling HJ, Kirch U, Zirbes TK, Rehm KE. Foreign–body reaction and the course of osteolysis after polyglycolide implants for fracture fixation: experimental study in sheep. J Bone Joint Surg Br 1996; 78: 369–376.
5. Witte F, Fischer J, Nellesen J, Crostack HA, Kaese V, Pisch A, Beckmann F, Windhagen H. In vitro and in vivo corrosion measurements of magnesium alloys. Biomaterials 2006; 27: 1013–1018.

6. Kraus T, Fischerauer SF, Hanzi AC, Uggowitzer PJ, Loffler JF, Weinberg AM. Magnesium alloys for temporary implants in osteosynthesis: in vivo studies of their degradation and interaction with bone. Acta Biomater 2012; 8: 1230-1238.
7. Chaya A, Yoshizawa S, Verdelis K, Myers N, Costello BJ, Chou DT, Pal S, Maiti S, Kumta PN, Sfeir C. In vivo study of magnesium plate and screw degradation and bone fracture healing. Acta Biomater 2015; 18: 262-269.
8. Wang H, Guan S, Wang Y, Liu H, Wang H, Wang L, Ren C, Zhu S, Chen K. In vivo degradation behavior of Ca-deficient hydroxyapatite coated Mg-Zn-Ca alloy for bone implant application. Colloids Surf B Biointerfaces 2011; 88: 254-259.
9. Kim SM, Jo JH, Lee SM, Kang MH, Kim HE, Estrin Y, Lee JH, Lee JW, Koh YH. Hydroxyapatite-coated magnesium implants with improved in vitro and in vivo biocorrosion, biocompatibility, and bone response. J Biomed Mater Res A 2014; 102: 429-441.
10. McBride ED. Absorbable metal in bone surgery. Bone Surg 1938; 111: 2464.
11. McCord CP PJ, Meek SF, Harrold GC. Chemical gas gangrene from metallic magnesium. Ind Med 1942; 11: 71-75.

12. Kuhlmann J, Bartsch I, Willbold E, Schuchardt S, Holz O, Hort N, Hoche D, Heineman WR, Witte F. Fast escape of hydrogen from gas cavities around corroding magnesium implants. Acta Biomater 2013; 9: 8714-8721.
13. Park JW, An CH, Jeong SH, Suh JY. Osseointegration of commercial microstructured titanium implants incorporating magnesium: a histomorphometric study in rabbit cancellous bone. Clin Oral Implants Res 2012; 23: 294-300.
14. Zhao SF, Jiang QH, Peel S, Wang XX, He FM. Effects of magnesium-substituted nanohydroxyapatite coating on implant osseointegration. Clin Oral Implants Res 2013; 24 Suppl A100: 34-41.
15. Hieu PD, Baek DH, Park DS, Park JT, Hong KS. Evaluation of stability changes in magnesium-incorporated titanium implants in the early healing period. J Craniofac Surg 2013; 24: 1552-1557.
16. Byun SH, Lim HK, Kim SM, Lee SM, Kim HE, Lee JH. The Bioresorption and Guided Bone Regeneration of Absorbable Hydroxyapatite-Coated Magnesium Mesh. J Craniofac Surg 2017; 28: 518-523.

17. Coelho PG, de Assis SL, Costa I, Thompson VP. Corrosion resistance evaluation of a Ca- and P-based bioceramic thin coating in Ti-6Al-4V. J Mater Sci Mater Med 2009; 20: 215-222.
18. Shadanbaz S, Dias GJ. Calcium phosphate coatings on magnesium alloys for biomedical applications: a review. Acta Biomater 2012; 8: 20-30.
19. Murugan R, Ramakrishna S. Bioresorbable composite bone paste using polysaccharide based nano hydroxyapatite. Biomaterials 2004; 25: 3829-3835.
20. Goodman SB, Yao Z, Keeney M, Yang F. The future of biologic coatings for orthopaedic implants. Biomaterials 2013; 34: 3174-3183.
21. Wong HM, Yeung KW, Lam KO, Tam V, Chu PK, Luk KD, Cheung KM. A biodegradable polymer-based coating to control the performance of magnesium alloy orthopaedic implants. Biomaterials 2010; 31: 2084-2096.
22. Van Oosterwyck H, Duyck J, Vander Sloten J, Van der Perre G, De Cooman M, Lievens S, Puers R, Naert I. The influence of bone mechanical properties and implant fixation upon bone

loading around oral implants. Clin Oral Implants Res 1998; 9: 407-418.

23. Du J, Lee JH, Jang AT, Gu A, Hossaini-Zadeh M, Prevost R, Curtis DA, Ho SP. Biomechanics and strain mapping in bone as related to immediately-loaded dental implants. J Biomech 2015; 48: 3486-3494.

24. Xu L, Yamamoto A. Characteristics and cytocompatibility of biodegradable polymer film on magnesium by spin coating. Colloids Surf B Biointerfaces 2012; 93: 67-74.

25. Zaky SH, Lee KW, Gao J, Jensen A, Close J, Wang Y, Almarza AJ, Sfeir C. Poly(glycerol sebacate) elastomer: a novel material for mechanically loaded bone regeneration. Tissue Eng Part A 2014; 20: 45-53.

26. Buijs GJ, van der Houwen EB, Stegenga B, Bos RR, Verkerke GJ. Mechanical strength and stiffness of biodegradable and titanium osteofixation systems. J Oral Maxillofac Surg 2007; 65: 2148-2158.

27. Gu X, Zheng Y, Cheng Y, Zhong S, Xi T. In vitro corrosion and biocompatibility of binary magnesium alloys. Biomaterials 2009; 30: 484-498.

28. Witte F, Kaese V, Haferkamp H, Switzer E, Meyer-Lindenberg A, Wirth CJ, Windhagen H. In vivo corrosion of four magnesium alloys and the associated bone response. Biomaterials 2005; 26: 3557-3563.
29. Huan ZG, Leeflang MA, Zhou J, Fratila-Apachitei LE, Duszczyk J. In vitro degradation behavior and cytocompatibility of Mg-Zn-Zr alloys. J Mater Sci Mater Med 2010; 21: 2623-2635.
30. Saldana L, Mendez-Vilas A, Jiang L, Multigner M, Gonzalez-Carrasco JL, Perez-Prado MT, Gonzalez-Martin ML, Munuera L, Vilaboa N. In vitro biocompatibility of an ultrafine grained zirconium. Biomaterials 2007; 28: 4343-4354.
31. Kulakov OB, Doktorov AA, D'Iakova S V, Denisov-Nikol'skii Iu I, Grotz KA. [Experimental study of osseointegration of zirconium and titanium dental implants]. Morfologiia 2005; 127: 52-55.
32. Diez M, Kang MH, Kim SM, Kim HE, Song J. Hydroxyapatite (HA)/poly-L-lactic acid (PLLA) dual coating on magnesium alloy under deformation for biomedical applications. J Mater Sci Mater Med 2016; 27: 34.
33. Viscasillas J, Seymour CJ, Brodbelt DC. A cadaver study

comparing two approaches for performing maxillary nerve block in dogs. Vet Anaesth Analg 2013; 40: 212-219.

34. Zhao L, Xu Z, Yang Z, Wang J, Wei X, Tang T, Zhao Z. Quantitative research using computed tomographic scanning of beagle jaws for determination of safe zones for micro-screw implantation. Ann Anat 2009; 191: 379-388.
35. Levesque J, Hermawan H, Dube D, Mantovani D. Design of a pseudo-physiological test bench specific to the development of biodegradable metallic biomaterials. Acta Biomater 2008; 4: 284-295.
36. Kannan MB, Raman RK. In vitro degradation and mechanical integrity of calcium-containing magnesium alloys in modified-simulated body fluid. Biomaterials 2008; 29: 2306-2314.
37. Liu D, Ding Y, Guo T, Qin X, Guo C, Yu S, Lin S. Influence of fine-grain and solid-solution strengthening on mechanical properties and in vitro degradation of WE43 alloy. Biomed Mater 2014; 9: 015014.
38. Zhang X, Yuan G, Niu J, Fu P, Ding W. Microstructure, mechanical properties, biocorrosion behavior, and cytotoxicity of as-extruded Mg-Nd-Zn-Zr alloy with different extrusion

ratios. J Mech Behav Biomed Mater 2012; 9: 153-162.

39. Gu XN, Zhou WR, Zheng YF, Cheng Y, Wei SC, Zhong SP, Xi TF, Chen LJ. Corrosion fatigue behaviors of two biomedical Mg alloys - AZ91D and WE43 - In simulated body fluid. Acta Biomater 2010; 6: 4605-4613.
40. Witte F. The history of biodegradable magnesium implants: a review. Acta Biomater 2010; 6: 1680-1692.
41. Zreiqat H, Howlett CR, Zannettino A, Evans P, Schulze-Tanzil G, Knabe C, Shakibaei M. Mechanisms of magnesium-stimulated adhesion of osteoblastic cells to commonly used orthopaedic implants. J Biomed Mater Res 2002; 62: 175-184.
42. Waizy H, Diekmann J, Weizbauer A, Reifenrath J, Bartsch I, Neubert V, Schavan R, Windhagen H. In vivo study of a biodegradable orthopedic screw (MgYREZr-alloy) in a rabbit model for up to 12 months. J Biomater Appl 2014; 28: 667-675.
43. Witte F, Abeln I, Switzer E, Kaese V, Meyer-Lindenberg A, Windhagen H. Evaluation of the skin sensitizing potential of biodegradable magnesium alloys. J Biomed Mater Res A 2008; 86: 1041-1047.
44. Yang JX, Cui FZ, Lee IS, Zhang Y, Yin QS, Xia H, Yang SX. In

vivo biocompatibility and degradation behavior of Mg alloy coated by calcium phosphate in a rabbit model. J Biomater Appl 2012; 27: 153-164.

45. Castellani C, Lindtner RA, Hausbrandt P, Tschegg E, Stanzl-Tschegg SE, Zanoni G, Beck S, Weinberg AM. Bone-implant interface strength and osseointegration: Biodegradable magnesium alloy versus standard titanium control. Acta Biomater 2011; 7: 432-440.
46. Hussain A, Takahashi K, Sonobe J, Tabata Y, Bessho K. Bone Regeneration of Rat Calvarial Defect by Magnesium Calcium Phosphate Gelatin Scaffolds with or without Bone Morphogenetic Protein-2. J Maxillofac Oral Surg 2014; 13: 29-35.
47. Webster TJ, Ergun C, Doremus RH, Bizios R. Hydroxylapatite with substituted magnesium, zinc, cadmium, and yttrium. II. Mechanisms of osteoblast adhesion. J Biomed Mater Res 2002; 59: 312-317.
48. Yamasaki Y, Yoshida Y, Okazaki M, Shimazu A, Kubo T, Akagawa Y, Uchida T. Action of FGMgCO3Ap-collagen composite in promoting bone formation. Biomaterials 2003; 24:

4913-4920.

49. Li Z, Gu X, Lou S, Zheng Y. The development of binary Mg-Ca alloys for use as biodegradable materials within bone. Biomaterials 2008; 29: 1329-1344.

50. Xu L, Yu G, Zhang E, Pan F, Yang K. In vivo corrosion behavior of Mg-Mn-Zn alloy for bone implant application. J Biomed Mater Res A 2007; 83: 703-711.

51. Lorenz C, Brunner JG, Kollmannsberger P, Jaafar L, Fabry B, Virtanen S. Effect of surface pre-treatments on biocompatibility of magnesium. Acta Biomater 2009; 5: 2783-2789.

52. Pietak A, Mahoney P, Dias GJ, Staiger MP. Bone-like matrix formation on magnesium and magnesium alloys. J Mater Sci Mater Med 2008; 19: 407-415.

53. Remennik S BI, Willbold E, Witte F, Shechtman D. New, fast corroding high ductility Mg-Bi-Ca and Mg-Bi-Si alloys, with no clinically observable gas formation in bone implants. Mater Sci Eng A 2011; 176: 1653-1659.

54. Xin Y, Hu T, Chu PK. In vitro studies of biomedical magnesium alloys in a simulated physiological environment: a review. Acta

Biomater 2011; 7: 1452-1459.

55. Alvarez-Lopez M, Pereda MD, del Valle JA, Fernandez-Lorenzo M, Garcia-Alonso MC, Ruano OA, Escudero ML. Corrosion behaviour of AZ31 magnesium alloy with different grain sizes in simulated biological fluids. Acta Biomater 2010; 6: 1763-1771.

56. Geng F, Tan LL, Jin XX, Yang JY, Yang K. The preparation, cytocompatibility, and in vitro biodegradation study of pure beta-TCP on magnesium. J Mater Sci Mater Med 2009; 20: 1149-1157.

57. Gray-Munro JE, Seguin C, Strong M. Influence of surface modification on the in vitro corrosion rate of magnesium alloy AZ31. J Biomed Mater Res A 2009; 91: 221-230.

58. Xu L, Zhang E, Yang K. Phosphating treatment and corrosion properties of Mg-Mn-Zn alloy for biomedical application. J Mater Sci Mater Med 2009; 20: 859-867.

59. Lim HK, Byun SH, Lee JY, Lee JW, Kim SM, Lee SM, Kim HE, Lee JH. Radiological, histological, and hematological evaluation of hydroxyapatite-coated resorbable magnesium alloy screws placed in rabbit tibia. J Biomed Mater Res B Appl Biomater

2016.

60. Drynda A, Seibt J, Hassel T, Bach FW, Peuster M. Biocompatibility of fluoride-coated magnesium-calcium alloys with optimized degradation kinetics in a subcutaneous mouse model. J Biomed Mater Res A 2013; 101: 33-43.
61. Hanzi AC, Gunde P, Schinhammer M, Uggowitzer PJ. On the biodegradation performance of an Mg-Y-RE alloy with various surface conditions in simulated body fluid. Acta Biomater 2009; 5: 162-171.
62. Imwinkelried T, Beck S, Iizuka T, Schaller B. Effect of a plasmaelectrolytic coating on the strength retention of in vivo and in vitro degraded magnesium implants. Acta Biomater 2013; 9: 8643-8649.
63. Tan L, Wang Q, Lin X, Wan P, Zhang G, Zhang Q, Yang K. Loss of mechanical properties in vivo and bone-implant interface strength of AZ31B magnesium alloy screws with Si-containing coating. Acta Biomater 2014; 10: 2333-2340.
64. Kim HW, Kim HE, Salih V, Knowles JC. Sol-gel-modified titanium with hydroxyapatite thin films and effect on osteoblast-like cell responses. J Biomed Mater Res A 2005; 74:

294-305.

65. Lee EJ, Lee SH, Kim HW, Kong YM, Kim HE. Fluoridated apatite coatings on titanium obtained by electron-beam deposition. Biomaterials 2005; 26: 3843-3851.

66. Meng X, Kwon TY, Yang Y, Ong JL, Kim KH. Effects of applied voltages on hydroxyapatite coating of titanium by electrophoretic deposition. J Biomed Mater Res B Appl Biomater 2006; 78: 373-377.

67. Park DS, Kim IS, Kim H, Chou AH, Hahn BD, Li LH, Hwang SJ. Improved biocompatibility of hydroxyapatite thin film prepared by aerosol deposition. J Biomed Mater Res B Appl Biomater 2010; 94: 353-358.

68. Rajesh P, Muraleedharan CV, Komath M, Varma H. Pulsed laser deposition of hydroxyapatite on titanium substrate with titania interlayer. J Mater Sci Mater Med 2011; 22: 497-505.

69. Faeda RS, Tavares HS, Sartori R, Guastaldi AC, Marcantonio E, Jr. Biological performance of chemical hydroxyapatite coating associated with implant surface modification by laser beam: biomechanical study in rabbit tibias. J Oral Maxillofac Surg 2009; 67: 1706-1715.

70. Ramires PA, Wennerberg A, Johansson CB, Cosentino F, Tundo S, Milella E. Biological behavior of sol-gel coated dental implants. J Mater Sci Mater Med 2003; 14: 539-545.
71. Kitabata H, Waksman R, Warnack B. Bioresorbable metal scaffold for cardiovascular application: current knowledge and future perspectives. Cardiovasc Revasc Med 2014; 15: 109-116.
72. Perkins J, Xu Z, Smith C, Roy A, Kumta PN, Waterman J, Conklin D, Desai S. Direct writing of polymeric coatings on magnesium alloy for tracheal stent applications. Ann Biomed Eng 2015; 43: 1158-1165.
73. Windhagen H, Radtke K, Weizbauer A, Diekmann J, Noll Y, Kreimeyer U, Schavan R, Stukenborg-Colsman C, Waizy H. Biodegradable magnesium-based screw clinically equivalent to titanium screw in hallux valgus surgery: short term results of the first prospective, randomized, controlled clinical pilot study. Biomed Eng Online 2013; 12: 62.
74. Yildiz M, Yildiz BS, Gursoy MO, Akin I. Recent developments in drug-eluting coronary stents. Cardiovasc Hematol Disord Drug Targets 2014; 14: 220-224.

Figure Legends

Figure 1. Pure Mg plates were designed (26x6x2 mm) for strength measurement.

A: Dimensions of the plate, B: Non-coated Mg plate (Non-coated Mg group), C: HA-coated Mg plate (HA-coated Mg group)

Figure 2. Intraoperative clinical photograph of a surgical technique for Mg plate insertion.

A: A transverse skin incision was made, and the periosteum was elevated using the periosteal elevator. B: The Mg plate was placed underneath the periosteum.

Figure 3. Comparison of flexural and tensile strength: A non-treated pure Mg plate versus a Ti plate.

A: The Ti plate has 2.5 times higher flexural strength than a Mg plate of the same thickness (0.6 mm) and 2.4 times higher than a Mg plate of 0.8mm thickness. B: The tensile strength of the Ti plate was more than 300 MPa, and that of the Mg plate was just over 100 MPa.

Figure 4. Retrieved Mg plate.

A: The corrosion products covered the surface of the non-coated Mg plates starting at 2 weeks. B: The HA-coated Mg plates showed no change until 2 weeks, but the coating started to strip off in a pin-point-like appearance at 4 weeks, which gradually progressed until 12 weeks.

Figure 5. Absorption pattern of plates in the HA-coated Mg group.

Absorption had a pin-point-like appearance until 8 weeks (white arrow). Absorption was progressed rapidly from 12 weeks.

Figure 6. Tensile strength and absorption rate of non-coated Mg and HA-coated Mg plates.

The tensile strength of the plates did not exceed 200 MPa. The HA-coated Mg plate showed statistically significant (p<0.001) resistance to absorption compared to the non-coated Mg group.

Figure 7. Dimensions and design of the ZK60 plates and screws.

Figure 8. Intraoperative clinical photograph of the LeFort I osteotomy canine model.

A: LeFort I osteotomy line was planned. B: LeFort I osteotomy was performed from the top of the piriform aperture to the second molar apex. C: Fixation of the four plates and 16 screws on each dog.

Figure 9. Postoperative clinical photographs after 2 weeks and 10 weeks.

A: The wound dehiscence that occurred at 2 weeks did not heal during the experimental period. B: The inflammatory symptoms continued after 2 weeks. C: All plates were not observed in all dogs. D: Only a few screw bodies fixed in the bone remained, and the screw heads were completely absorbed after 10 weeks.

Figure 10. Design and dimensions of the plates and screws (WE43 and Ti).

A: Extruded WE43 plates and screws, B: Ti plates and screws

Figure 11. Intraoperative clinical photograph of the fixation of plates and screws.

Four plates and 16 screws were fixed. A: Extruded WE43 plates and screws, B: Ti plates and screws

Figure 12. The position of the plate as seen in the μCT image.

Figure 13. Cell attachment of pure Mg and WE43.

The pre-incubated cell (pre-osteoblast cell line: MC3T3-E1) response was evaluated after one day of culturing by observing the attached cells with SEM (x1000). There was no difference in cell attachment between pure Mg and WE43.

A: Pure Mg, after 6 hours, B: Pure Mg, after 24 hours, C: WE43, after 6 hours, D: WE43, after 24 hours

Figure 14. Absorption rate of WE43 for 60 days.

Static immersion tests in simulated body fluid (SBF) were performed at a pH of 7.35 and 37.0°C. The absorption was slow compared to that of ZK60. Approximately 60% of the initial mass remained at 60 days.

Figure 15. Postoperative clinical photograph after 24 weeks.

No dehiscence was observed intraorally until 24 weeks after operation. A: Experimental group (WE43), B: Control group (Ti)

Figure 16. Clinical evaluation of the experimental group (WE43).

A: Gas formation was observed starting at 8 weeks. B: Infraorbital fistula was observed in three dogs at 12 weeks. C: The fistula gradually decreased and disappeared by 24 weeks.

Figure 17. Radiological evaluation of the experimental group (WE43).

Gas formation was observed in three of the experimental dogs at 12 weeks and was not observed at 24 weeks. All of the plates in the experimental group were well maintained until 12 weeks and were mostly absorbed at 24 weeks.

Figure 18. Radiological evaluation of the experimental group (WE43).

Two dogs showed less gas formation at 12 weeks compared to other dogs. The plates were completely absorbed at 24 weeks in

these two dogs. The LeFort I osteotomy line in the experimental group disappeared by 24 weeks.

Figure 19. Radiological evaluation of the control group (Ti).
Plates and screws were maintained in their initial position without any problems in all dogs.

Figure 20. Histologic findings after 24 weeks (scale bar=1000 ㎛).
New bone (black arrow) was formed near the screw head and covered the screw body in both groups. Histologic examination showed no specific differences between the experimental group and the control group. A, B: Experimental group (WE43 plate), C, D: Control group (Ti plate)

Figures

Figure 1.

Figure 2.

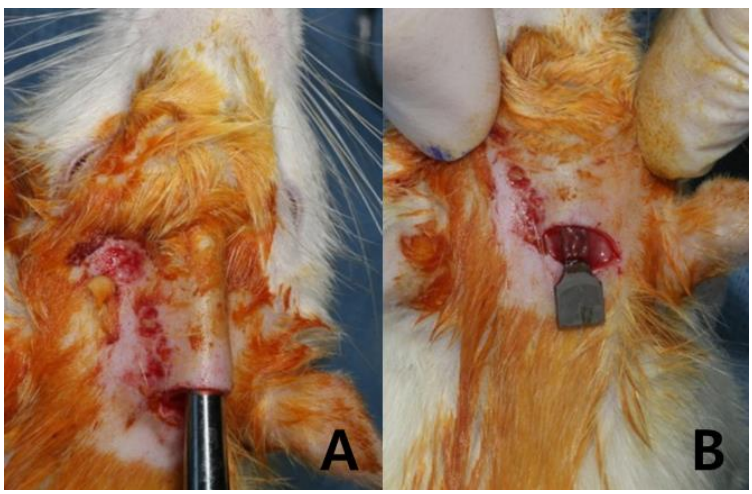

Figure 3.

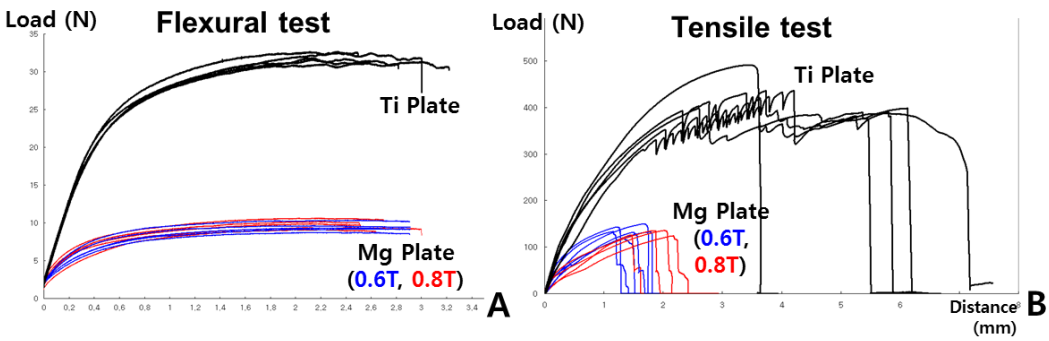

Figure 4.

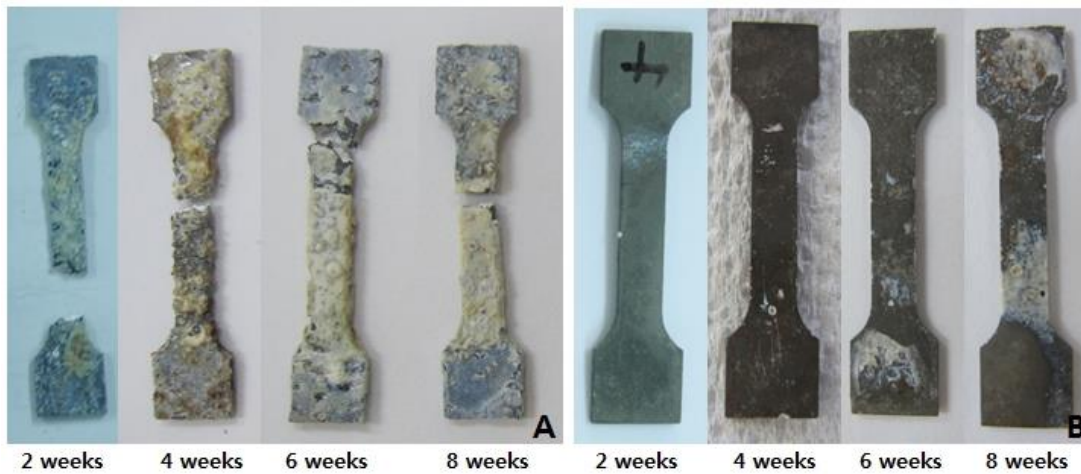

Figure 5.

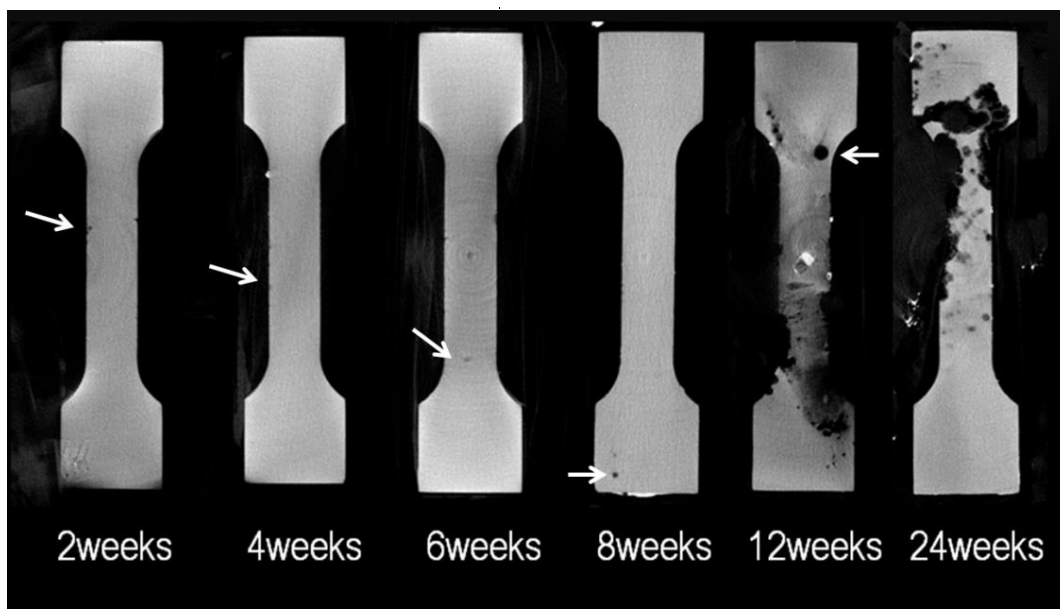

Figure 6.

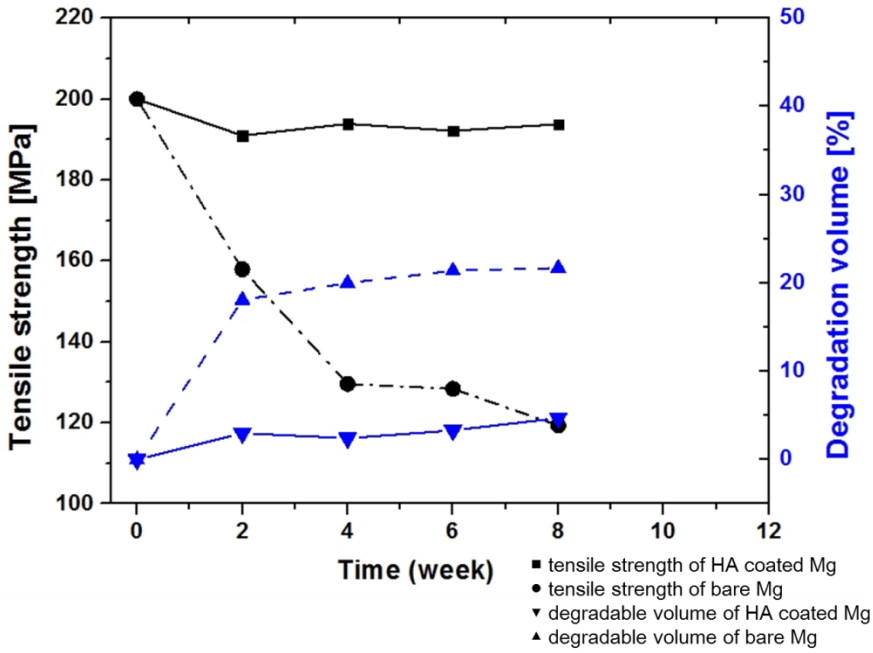

Figure 7.

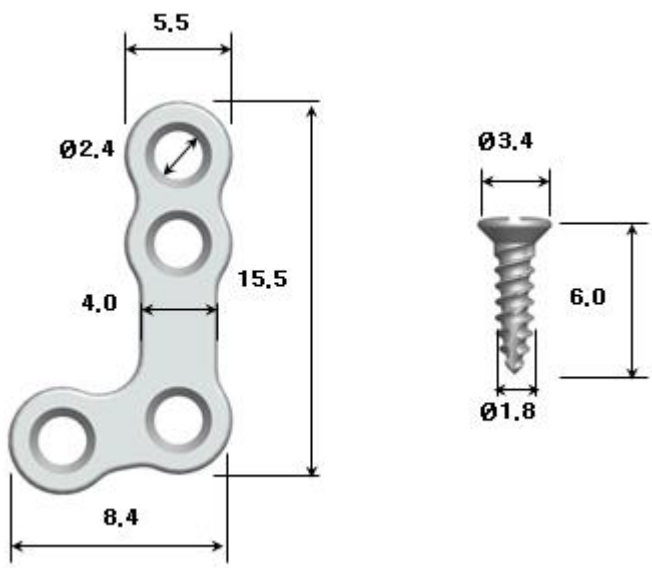

Figure 8.

Figure 9.

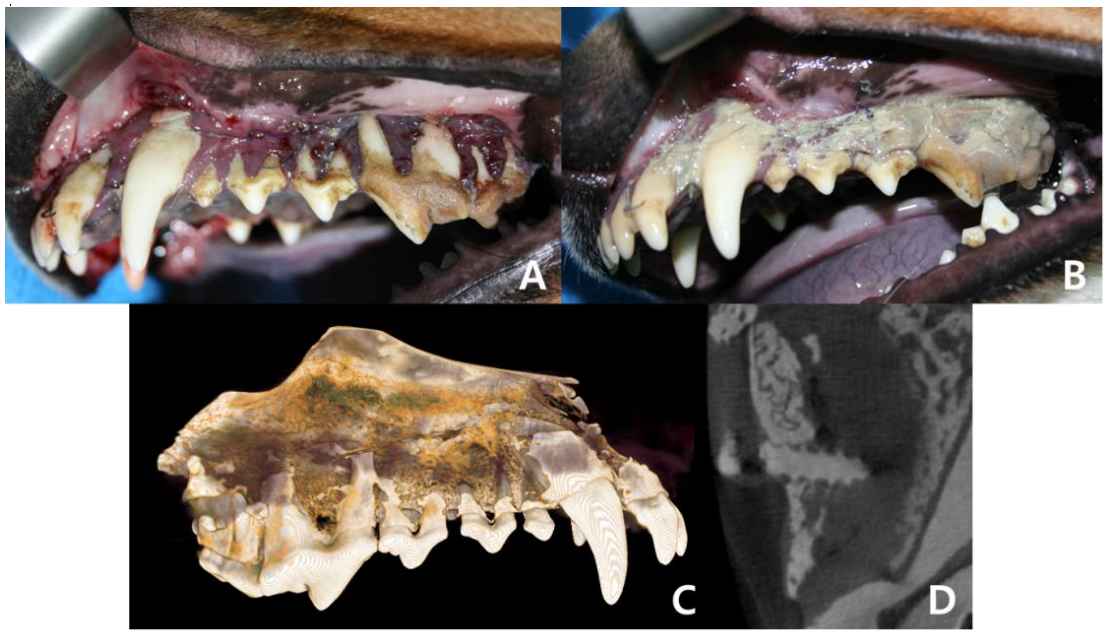

Figure 10.

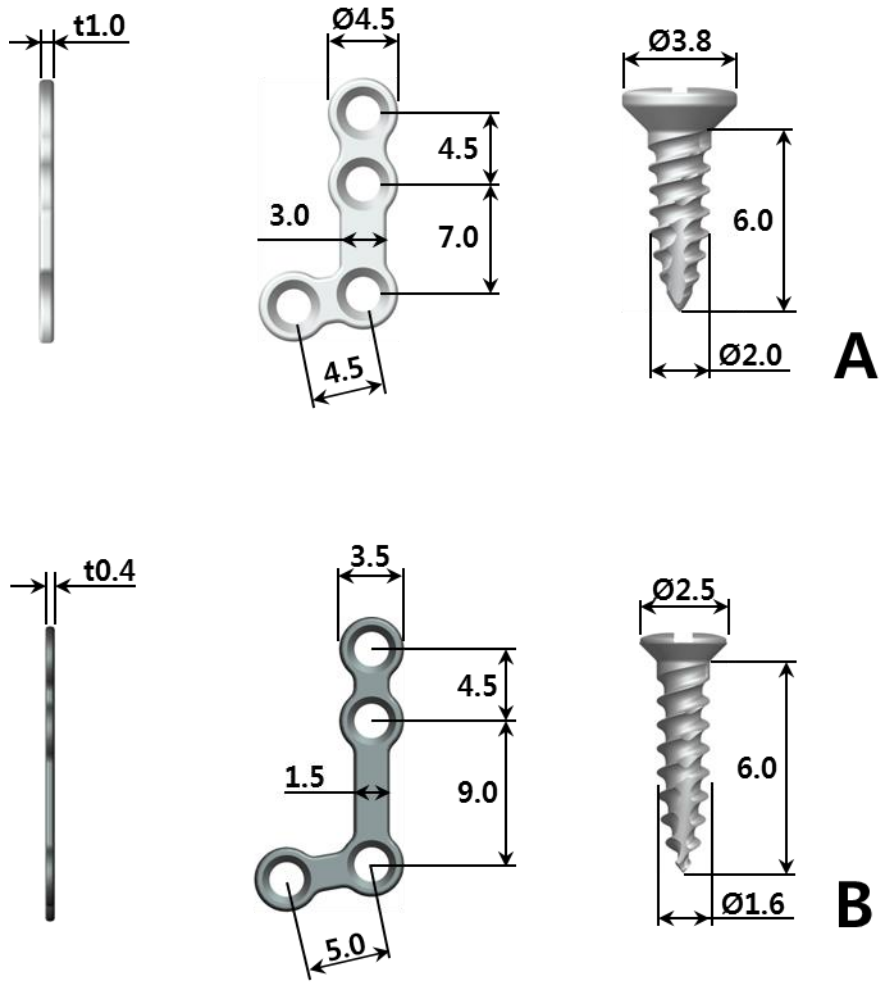

Figure 11.

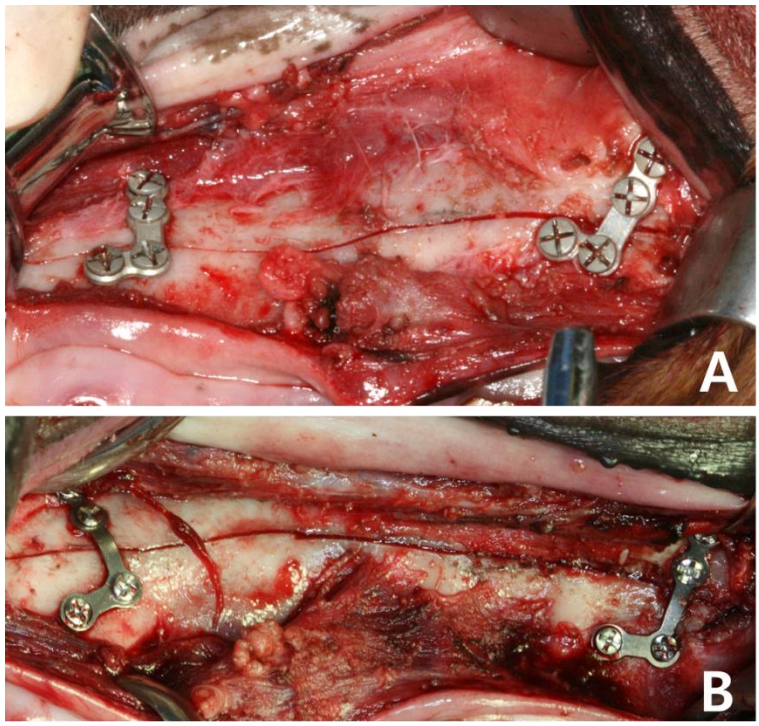

Figure 12.

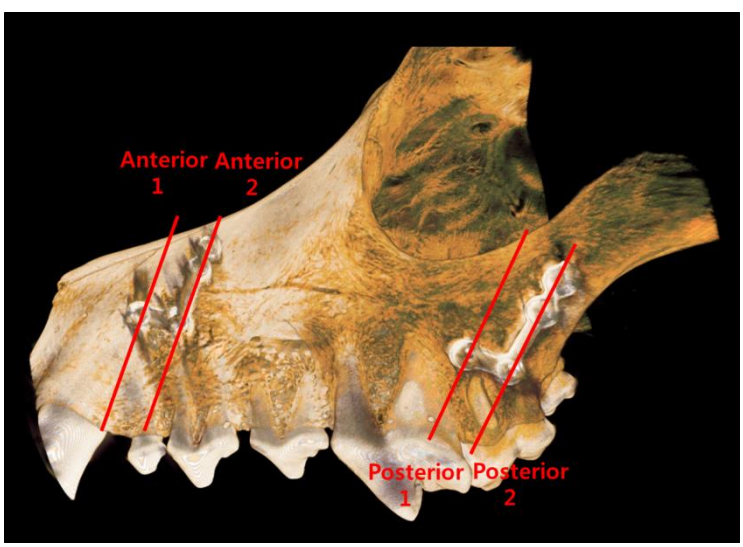

Figure 13.

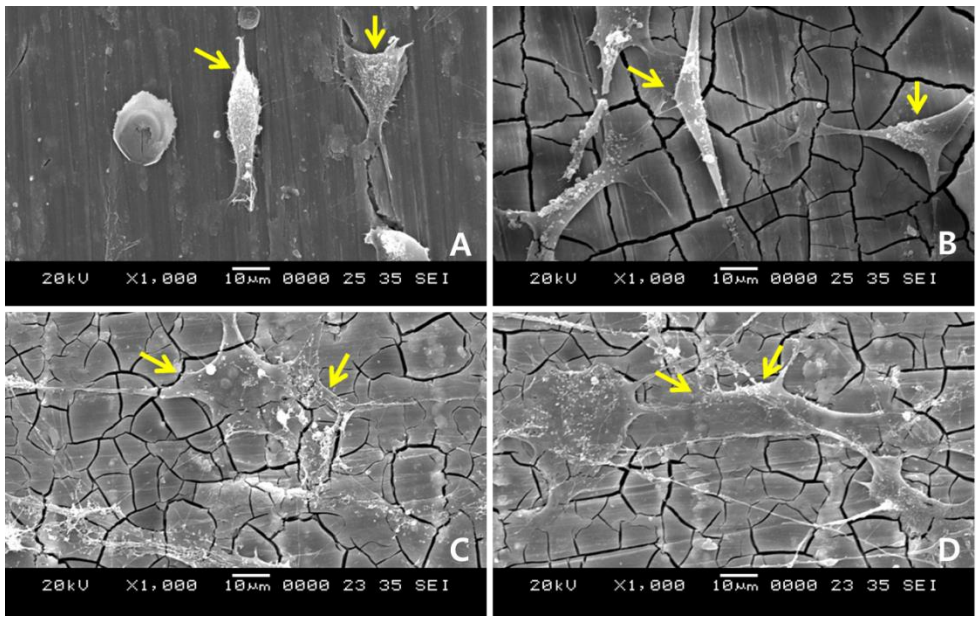

Figure 14.

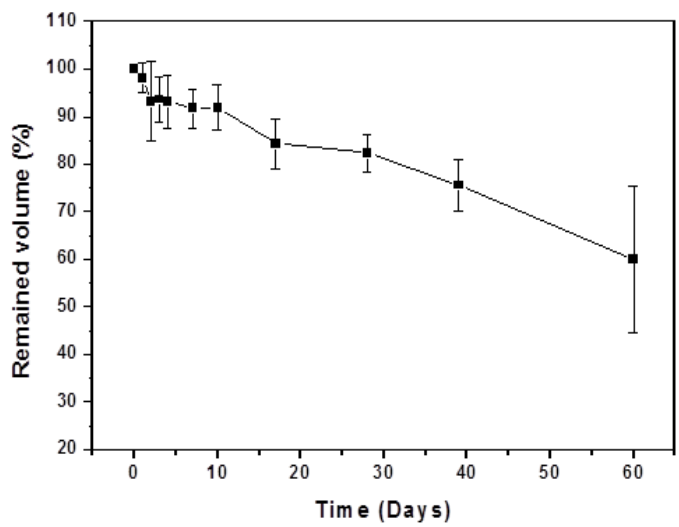

Figure 15.

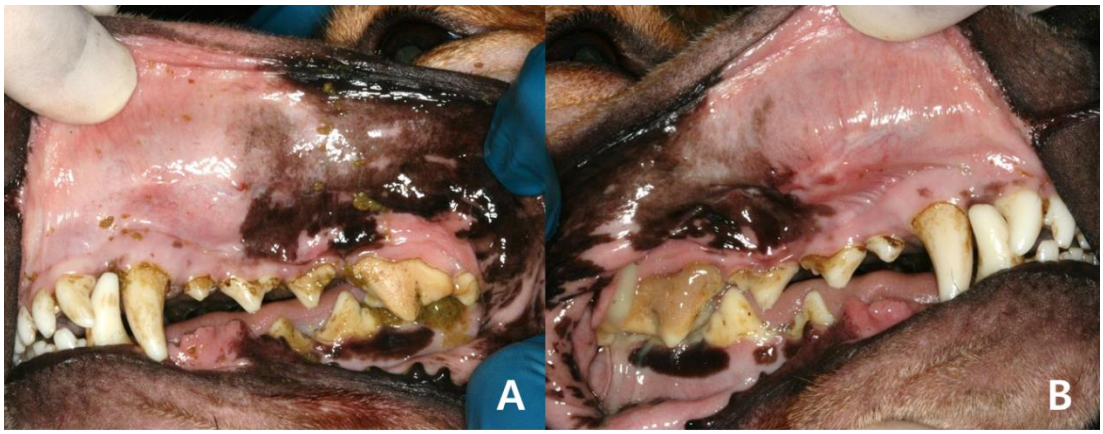

Figure 16.

Figure 17.

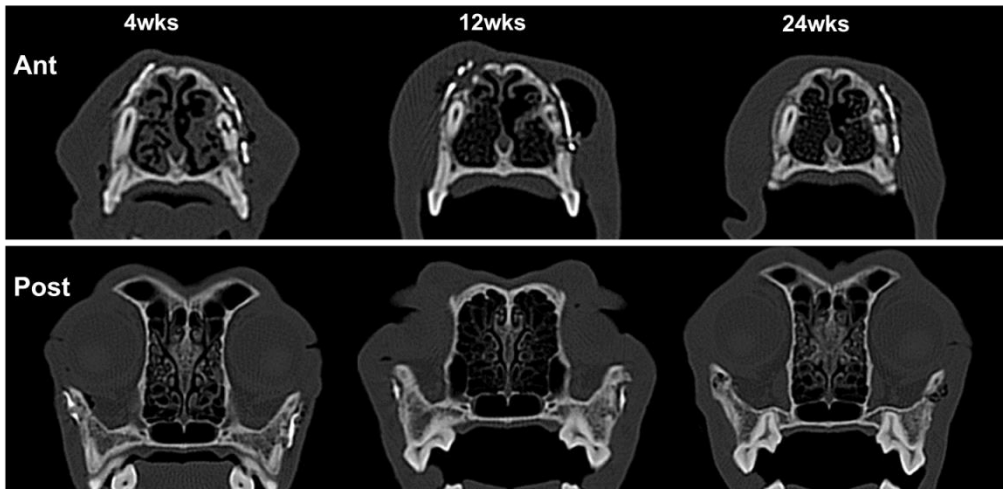

Figure 18.

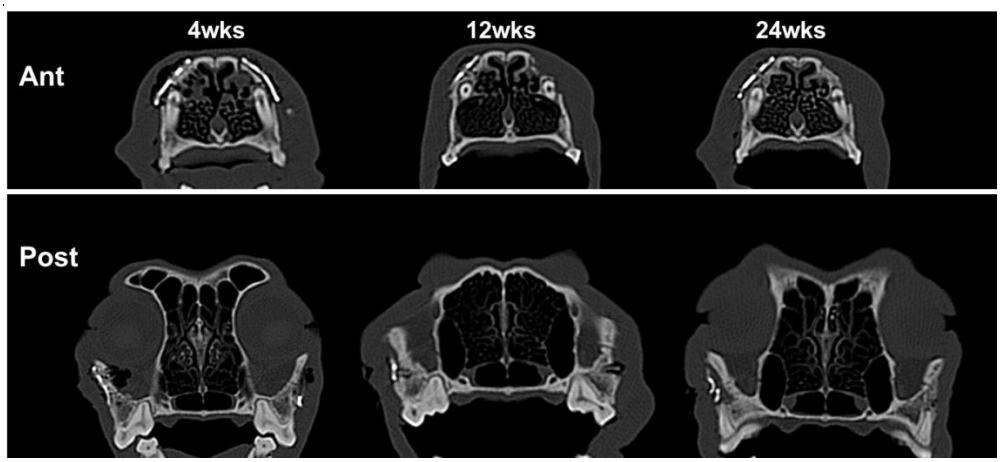

Figure 19.

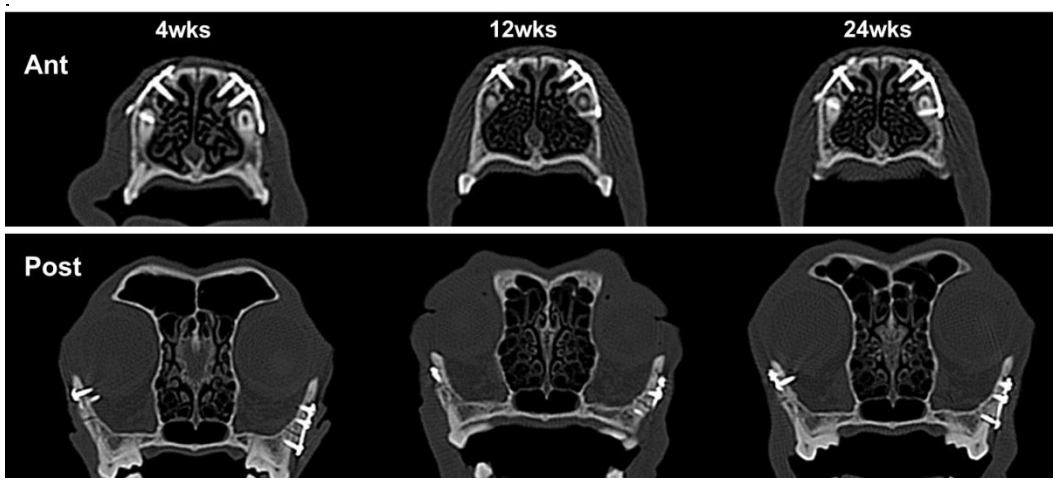

Figure 20.

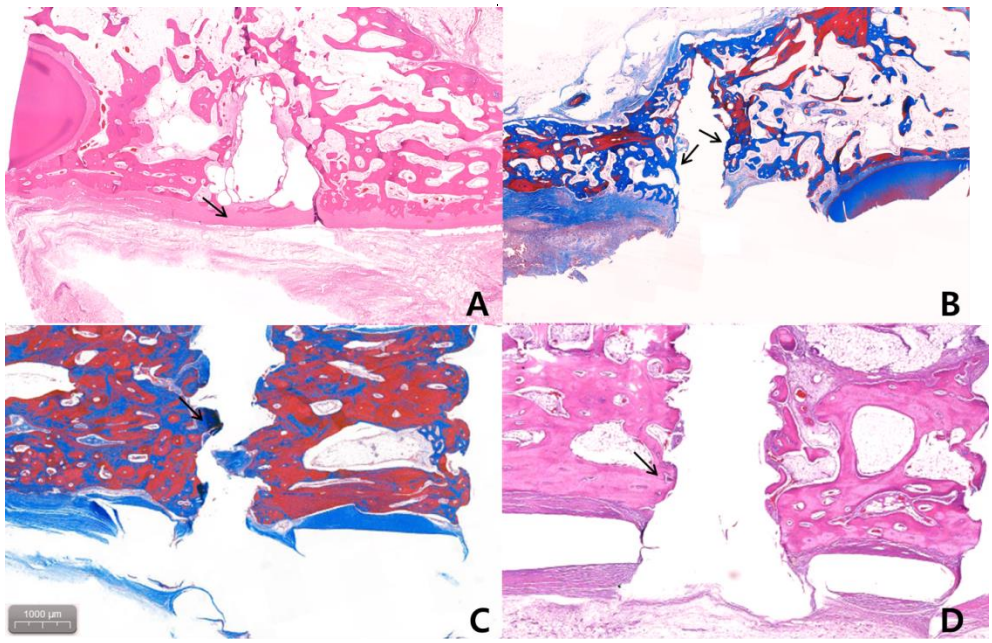

Tables

Table 1. Chemical composition of Mg alloy (ZK60 and WE43)

ASTM No.	Mg (min)	Al	Ca	Cu	Fe	Li	Mn	Nd	Ni	1)R.E.	Si	Y	Zr	Zn	Other Impurities	
															each	total
ZK60	Bal.	0.0014	...	0.001	0.0021		0.012		...		0.0016		0.64	4.8-6.2		0.3
WE43	Bal.	...	...	0.02	0.01	0.2	0.03	2.0-2.5	0.005	1.9	...	3.7-4.3	0.4-1.0		0.01	...

1)R.E : Rare Earth Ref. : ASTM B 107

[unit : wt.%]

Table 2. Improved mechanical properties of extruded WE43

ASTM No.	Tensile strength(㎫)	Tensile yield strength(㎫)	Elongation (%)
ZK60	328	251	15
WE43	260	160	6
Extruded WE43	303	195	6

Abstract in Korean

국문초록

마그네슘 소재 흡수성 뼈고정판 개발

변 수 환

서울대학교 대학원 치의과학과 박사과정 구강악안면외과학 전공

(지도교수 이 종 호)

배경 및 연구 목적

현재 많이 사용되고 있는 티타늄 (Ti)으로 만들어진 뼈고정 장치는 우수한 기계적 물성과 생체 적합성을 가지고 있지만 체내에서 흡수가 되지 않아 장기적으로 감염, 노출등과 같은 합병증 발생가능성이 있어 필요시 추가적인 수술을 통해 제거가 요구된다. 폴리머로 만들어진 뼈고정 장치는 생체내에서 분해되기 때문에 제거할 필요가 없으나 기계적 강도가 티타늄에 비해 부족하다는 단점이 있다.

티타늄과 폴리머와는 달리 마그네슘 (Mg)은 체내 분해와 강도면에서 장점을 가지고 있다. 마그네슘은 체내에서 분해가 되어 장기간 감염 가능성을 줄이고 추가적인 제거 수술이 필요하지 않으며 뼈치유를

촉진한다. 이러한 이유로 마그네슘은 두개악안면영역과 정형외과에서 연구되고 있다. 그러나 마그네슘의 빠른 흡수는 과도한 수소가스 발생을 야기해 임상적 사용을 어렵게 한다. 또한 마그네슘의 강도는 폴리머보다는 높지만 아직 티타늄보다는 부족하다는 단점도 가지고 있다.

본 연구의 목적은 이러한 마그네슘 재료의 강도 증진과 흡수 속도 조절을 통하여 두개악안면부 임상 적용이 가능한 흡수성 뼈고정판을 개발하고자 함이다.

연구 방법

1장: 강도가 향상된 순수 마그네슘 판의 개발 및 평가

티타늄 판과 가공하지 않은 순수 마그네슘 판의 인장 강도와 굽힘 강도를 평가하였다. 생체 내 실험에 사용된 순수 마그네슘은 2축 압연 가공에 의해 기계적 강도가 향상되었다. 순수 마그네슘 판을 쥐의 두개뼈 상방에 삽입했다. 대조군 (non-coated Mg, 코팅되지 않은 군)에서는 순수 마그네슘 판을 25개체 쥐에 적용하고 2주, 4주, 6주, 8주 및 12 주에 각각 5개체씩 희생시켰다. 실험군 (HA-coated Mg, 코팅된 군)에서는 수산화인회석 (HA) 코팅된 마그네슘 판을 30개체 쥐에 적용하고 2주, 4주, 6주, 8주, 12주, 및 24주에 5개체씩 희생시켰다. 희생시 염증, 감염, 수소 가스 형성, 수술 부위 열개 및 마그네슘 판의 노출 여부를 관찰하였다. μCT 촬영 후 적출한 마그네슘 판의 흡수양상

및 인장 강도를 평가하였다.

2장: 마그네슘 합금 뼈고정판의 개발 및 평가–ZK60

합금은 순수 마그네슘의 기계적 강도를 향상시킬 수 있는 좋은 방법이다. 순수 마그네슘의 기계적 강도 한계를 극복하기 위해 강도가 큰 ZK60을 선택하였다. 체액내에서 빠른 흡수가 예상되어 흡수 속도를 늦추기 위해 PLLA 코팅을 시행하였다. PLLA 코팅된 ZK60 뼈고정판은 LeFort I osteotomy canine model에서 평가되었다. 총 2개체의 개에서 각각 4개의 L형 뼈고정판을 16개의 고정 나사로 전후방 지지대에 고정하였다. 수술 부위 열개, 뼈고정판 노출, 가스 형성, 교합 관계, 염증, 고름 형성, 음식 섭취, 누공 형성을 매주 평가하였다. 10주 후에 2마리 모두 희생시키고, μCT 촬영을 통해 가스 형성 여부, 뼈고정판과 고정 나사의 흡수율을 평가하였다.

3장: 마그네슘 합금 뼈고정판의 개발 및 평가–WE43

ZK60은 적절한 기계적 강도를 가지고 있지만 흡수 속도가 빠르다. 그래서 흡수 속도가 느린 다른 재료로의 변경이 요구되었다. WE43은 ZK60보다 기계적 강도가 낮으나 느린 흡수 속도를 가지고 있다. 그러나 임상적으로 적용하기에는 기계적 강도가 낮아 강도를 향상시킬 수 있는 추가적인 가공 공정이 요구되었다. 압출 가공 공정을 통해 WE43

마그네슘 합금 강도를 증진시켰다. WE43의 생체적합성은 전조골 세포 (pre-osteoblast cell line, MC3T3-E1)을 이용하여 평가하였다. 그리고 모의 체액 (SBF)에서 60일 이상의 기간 동안 분해 속도를 조사하였다. 티타늄 뼈고정판, 순수 마그네슘 뼈고정판, WE43 뼈고정판의 3점 굽힘 강도와 인장 강도를 평가하였다.

압출 가공된 WE43은 LeFort I osteotomy canine model에서 평가하였다. 총 10개체의 개를 실험군 5개체와 대조군 5개체로 나누었다. 임상 평가는 ZK60에서의 평가와 동일하게 시행하였다. μCT는 4주, 12주, 24주에 촬영하였으며. 뼈고정판의 흡수와 주위 뼈 변화를 평가하였다. 24주에 희생한 후 조직학적 평가를 시행하였다.

연구 결과

1장: 강도가 향상된 순수 마그네슘 판의 개발 및 평가

마그네슘 판은 티타늄 판보다 낮은 굽힘 강도 및 인장 강도를 보였다. 대조군 (non-coated Mg, 코팅되지 않은 군)에서는 가스 형성과 마그네슘 판의 노출이 2주부터 관찰되었다. 실험군 (HA-coated Mg, 코팅된 군)에서는 12주까지 가스 형성이 관찰되지 않았으나 24주 이후에 형성되기 시작하였다. 수산화인회석으로 코팅된 실험군은 대조군에 비해 느린 흡수를 보였으며 12주까지 인장 강도가 유지되었다(>190 MPa).

2장: 마그네슘 합금 뼈고정판의 개발 및 평가-ZK60

2개체 모두 수술 과정 중 특별한 문제가 없었으며 수술 후 뼈고정판의 노출, 가스 형성, 누공 형성, 교합 변화는 관찰되지 않았다. 그러나, 수술 2주 후에 발생한 수술 부위 열개는 실험 기간 동안 치유되지 않았다. 염증 증상은 2주 이후 지속되었으며 10주 후 모든 뼈고정판은 관찰되지 않았고 뼈 내부에 고정된 일부 고정 나사만 관찰되었다.

3장: 마그네슘 합금 뼈고정판의 개발 및 평가-WE43

순수 마그네슘과 WE43 사이의 세포 부착 정도는 차이가 없었다. 60일동안 WE43의 흡수 속도는 일정하게 유지되었으며 ZK60에 비해 느리게 나타났다. 60일 후에 약 60%정도 남았으며 굽힘 강도 및 인장 강도는 압출 가공된 WE43가 그렇지 않은 WE43보다 높았다.

수술 후 8주부터 실험군 3개체에서 부종 및 가스 형성이 관찰되었다. 수술 후 12주부터 실험군 3개체에서 누공 및 염증 증상이 관찰되었으며, 이는 24주까지 점차적으로 감소하고 사라졌다. 뼈로부터 분리된 마그네숨 합금 뼈고정판은 빠른 흡수를 보였으나, 뼈 내부에 고정된 고정 나사는 느린 흡수를 보였다. 실험군 2개체는 다른 개체와 비교하여 12주에 가스 형성이 적게 관찰되었다. 이러한 2개체는 24주에 마그네슘 합금 뼈고정판이 완전히 흡수되었고, 가스가 거의 관찰되지 않았다.

대조군에서는 모든 개체에서 티타늄 판과 고정 나사가 아무런 문제없이 처음 위치에 잘 유지되었다. 모든 실험 개체에서 조골 세포대가 고정 나사 주위에서 관찰되었으며 새로운 뼈가 뼈고정판과 고정 나사 주위에 잘 형성되었다. 조직학적 소견은 실험군과 대조군 사이 별다른 차이점이 관찰되지 않았다.

결론

순수 마그네슘의 기계적 강도를 2축 압연 가공을 통해 향상시켰지만 인장 장도는 200 MPa을 넘지 못했다. ZK60의 인장 강도는 300 MPa를 넘었지만 빠른 흡수로 인해 임상 적용이 불가능하다고 판단되었다. 압출 가공된 WE43의 강도는 중안모 적용에 충분하다. WE43는 흡수 과정에서 가스가 형성된다는 단점이 있었지만, 코팅과 같은 표면 처리를 이용한 흡수 속도 조절을 통해 해결될 수 있다고 생각한다. 이러한 결과를 토대로 적절하게 처리된 WE43 마그네슘 합금으로 제작된 뼈고정판은 임상적으로 적용 가능하다고 판단된다.

주요어: 흡수성판, 마그네슘, 뼈고정판, 기계적 강도, 마그네슘 합금, ZK60, WE43, 생체친화성

학번: 2012-31175